MODELING AND DYNAMIC ANALYSIS OF MULTI-SPOOL ROTOR SYSTEMS

by

YOGESH KUMAR

DEPARTMENT OF MECHANICAL ENGINEERING

INDIAN INSTITUTE OF TECHNOLOGY, KANPUR

February, 2001

MODELING AND DYNAMIC ANALYSIS OF MULTI-SPOOL ROTOR SYSTEMS

A Thesis Submitted
in Partial Fulfillment of the Requirements
for the Degree of

MASTER OF TECHNOLOGY

February 2001

by

YOGESH KUMAR

Department of Mechanical Engineering

INDIAN INSTITUTE OF TECHNOLOGY

KANPUR – 208016 (INDIA)

CERTIFICATE

It is certified that the work contained in the thesis entitled "**Modeling and Dynamic Analysis of Multi-Spool Rotor Systems**" by *Yogesh Kumar* has been carried out under my supervision and that this work has not been submitted elsewhere for a degree.

Nalinaksh Vyas.

Dr. Nalinaksh S Vyas
(Professor)
Department of Mechanical Engineering,
Indian Institute of Technology, Kanpur.

February 2001

ACKNOWLEDGEMENTS

I wish to express my profound gratitude and indebtedness towards my thesis supervisor Dr. N.S. Vyas for his inspiring guidance, invaluable suggestions and constant encouragement. His openness and grant of adequate freedom to me for thesis work kept my thought process unbridled

I am extremely thankful to Animesh, Nivea, Sunil, Prashanth and Lt. Dhiroj who devoted their valuable time and helped me in all possible ways towards successful completion of my thesis work. I appreciate and extend my thanks to Mr. J.P. Verma for his untiring help. I thank all those who have contributed directly or indirectly to my thesis.

I would like to thank all my friends for making my stay at IITK very enjoyable and memorable. I will cherish the moments forever.

Indian Institute of Technology, Kanpur. Yogesh Kumar

February 2001

ABSTRACT

Dual and multi-spool rotors are being increasingly used in large output compressors and turbines. In such applications the rotor size becomes large, which leads to increase in shaft flexibility and associated problems. In order to overcome this constraint and to get additional advantages single rotors are converted to twin or multi-spool rotor systems, whereby shafts are made hollow to support other shafts through inter shaft bearing(s) The focus of the present study is to model such shaft-disc-bearing configurations for rotordynamic analysis. Transfer matrix approach has been adopted to develop the analytical model and programming is done using MATLAB. In addition Finite Element models have been developed using NISA package. Free vibration analysis, including estimation of natural frequencies, mode shapes, critical speeds for backward and forward whirls and unbalance response analysis including whirl orbit computation and beat phenomenon have been carried out. Standard problems available in literature are considered and results obtained through both procedures are compared to validate the models. Transfer matrix and FEM models have also been developed for a typical two-spool multi-stage aeroengine rotor using sample geometric, material and bearing data.

CONTENTS

NOMENCLATURE

A	Overall transfer matrix for eigenvalue calculation
$[Be]$	Junction matrix
$[\boldsymbol{Be}]$	Bearing matrix
$C_{zz}, C_{yy}, C_{zy}\ C_{yz}$	Bearing damping coefficient
e_i	Eccentricity for the ith unbalance
E	Young's modulus
F_k	Total elastic force on kth ball of all bearing
[F]	Field matrix
I_P	Polar Inertia
I_T	Diametral Inertia
[I]	Unit matrix
k	Spring stiffness
K_n	Coefficient of proportionality
$K_{zz}, K_{yy}, K_{zy}, K_{yz}$	Bearing stiffness coefficient
l_i	Length of shaft segment
m_i	Mass of at ith station
M_y, M_z	Moment in the x-z, x-y plane
$M_{yc}, M_{ys}, M_{zc}, M_{zs}$	Cosine and sine terms of M_y and M_z
[P]	Point matrix
p	Critical speed
R_y, R_z	Reaction force at bearing in y and z direction respectively
{S}	State vector
T_y, T_z	Gyroscopic couple in x-y and x-z plane
u_i	ith unbalance
[U]	Over all transfer matrix
v	Displacement in z direction

V_y, V_z	Shear force along the y and z axis
$V_{yc}, V_{ys}, V_{zc}, V_{zs}$	Cosine and sine component of V_y and V_z
w	Displacement in y direction
Z_{bi}	Impedance of ith bearing
ω	Operating speed
θ	Slope in x-z plane
ϕ	Slope in x-y plane
μ	Ratio of cross and direct stiffness $K_{yz}/K_{yy}, K_{zy}/K_{zz}$
δ	Deflection or contact deformation
δ^*	Dimension less contact deformation
δ_k	Deflection at kth ball in ball bearing
η_k	Angle between the line of action of radial load and the radius passing through the center of the kth rolling body in bearing
$\Sigma\sigma_{i,o}$	Curvature sum for inner and outer raceway
$\partial\sigma_{i,o}$	Curvature difference for inner and outer raceway

SUPERSCRIPTS

L	Left side of station
R	Right side of station

LIST OF FIGURES

LIST OF TABLES

CHAPTER 1

INTRODUCTION

More than ninety percent of machinery used in industry can be categorized as rotating machines. Some of them are steam and gas turbines, compressors, turbogenerators, aeroengines etc. These are typical multimass rotor installations and comprise of mechanical elements like shafts, discs, blades, seals, couplings, gears etc. The basic model is constituted of a shaft carrying one or more than one disc. The arrangement may be supported in rolling element or in fluid film bearings.

In case of large output compressors and turbines, the rotor size becomes large, which leads to increase in shaft flexibility and other associated problems. In order to overcome this constraint and to get additional advantages a single rotor is converted to a twin or multi-spool rotor system, whereby shafts are made hollow to support other shafts, through inter shaft bearing(s). Such rotor systems are widely used in aeroengines, where various compressor and turbine stages (LP, IP, HP) are combined together to form a set of inner and outer rotors. A dual compressor aeroengine utilizes two separate compressors, each with its own driving turbine. One of the principle advantages of the split compressor in aeroengine is greater flexibility of operation without danger of stall. The low-pressure compressor can operate at the best speed for accommodation of the low pressure, low temperature at the forward part of engine. The high-pressure compressor is speed governed to operate at the proper speed for most efficient performance. Use of dual compressor makes it possible to attain pressure ratio of more than 13:1, where single axial compressor produce pressure ratio of 6 or 7:1.

This type of rotor system minimizes shaft deflections caused by rotor unbalance and improves engine efficiency, performance and reliability by eliminating the static support structure in the aerodynamic flow. It also facilitates easy mounting with engine casing and provides compactness to the overall structure.

However, the intershaft bearing(s) becomes a source of cross-excitation between the two shafts. This cross-excitation makes the mathematical treatment of dual rotor system different from that of single rotor. Cross-exciting vibration between inner and outer shafts is effected through the intershaft bearing and thus the dynamic response of one rotor also depends upon the dynamic behavior of the other.

The present study is an attempt in rotor dynamic modeling and analysis of two/multi-spool rotors. Rotor dynamics has been an area of extensive investigation in the past. Two distinct approaches for analysis of multimass rotors have been the continuous systems approach and the discrete systems approach. In continuous systems approach the mass and stiffness properties are taken to be distributed continuously along the shaft. This method is used in finite element method with component mode synthesis to solve dual rotor or large system problem. In discrete systems approach mass and stiffness properties are discretized and matrix methods are generally employed to obtain system response. The finite element method has a distinct advantage in assembling the elemental equation with out any recourse to intershaft bearing conditions as in the case of transfer matrix method. Dimentberg (1961) gave an exhaustive treatment to the transverse vibration of rotating shafts through a continuous system approach. Tondl (1965) analyzed various aspects of rotor dynamics, like critical speeds, stability, self excited vibrations, fluid film bearing characteristics etc. Another text on the subject is by Rao (1996) who bases his treatment on the discrete system approach, specifically transfer matrix methods of Myklestad (1944) and Prohl (1945). Some salient studies on various aspects of rotor dynamics are - Jeffoct on unbalance response of single mass rotors, Kikuchi (1970), on vibration of multi-disc and multi-bearing rotor systems; Green (1958) and Carnegie (1964), on gyroscopic effects; Smith (1969), Lund (1965) and Morton, Johnson and Wale (1988) on fluid film bearings. Goodwin (1955) has carried out extensive experimental studies for the determination of bearing coefficients, which are eight in number. He has presented his results in the form of graphs and charts. Lalanne (1985) has reviewed vibration problems of jet engines. Childs (1976) developed a modal simulation model based on eigendata at zero running speed, accounting for gyroscopic effects, bearing damping and nonlinearities, structural modal damping and concentrated damping due to squeeze film dampers. Glasgow and Nelson (1979) applied component mode synthesis

and showed that significant reduction in the size of the problem is achieved while still retaining the essential dynamic characteristics of the lower modes. Other analysis using finite element method have been done by Berthier et al. (1985) and using component mode synthesis by Li and Gunter (1982). Zeng and Hu (1988) use gyroscopic mode synthesis technique for multishaft rotor-bearing case system. Squeeze film dampers play an important role in multi spool aeroengine rotor system. Studies on stability aspects using intershaft squeeze film damper in two spool rotor system have been carried out by several authors, Hibner, Bansal and Buono (1978), Li and Hamilton (1986) and by El Shafei (1991). Hibner et al. (1977, 1978) investigated the stability behavior of dual rotor system with squeeze film damper and suggested means for controlling the instability by changing the stiffness of the intershaft bearings by adding the spring in parallel. The transfer matrix method has been applied in various forms to solve multi spool rotor system problems. Hibner (1974) applied a unique transfer matrix method to an idealized equivalent engine system for predicting vibratory response accounting for nonlinear viscous damping effects. Another analysis has been by Bansal and Kirk (1975) for stability and damped critical speeds. Kazao and Gunter (1989a) have also studied energy distributions in the rotor system and have shown its utility in designing effective bearings and dampers. Gupta et al. (1988) presented a theoretical formulation to determine the steady state unbalance response of dual rotor system with a flexible intershaft bearing using extended transfer matrix method, where the extended transfer matrix assumed a dimension of 33x33. Transfer matrix impedance coupling method developed by Taiping (1988) is useful to find eigensolutions of multi-spool rotor system.

Present Work

The focus of the present work is to develop models for dynamic analysis of two and multi-spool rotors. The modeling involves (i) free vibration analysis - including estimation of natural frequencies, mode shapes, critical speeds for backward and forward whirls and (ii) unbalance response analysis including whirl orbit computation and beat phenomenon. Models have been developed through (i) transfer matrix approach with programming being done in MATLAB and (ii) Finite Element procedure using NISA

FEM package version 7.0. Standard problems available in literature are considered and results obtained through both procedures are compared to validate the models. Features such as the nature of the steady state orbit, cross excitation between the rotors, critical speeds and mode shapes are discussed. Free vibration modeling procedure is discussed in Chapter 2, while unbalance response analysis is discussed in Chapter 3. In addition the modeling exercise has been extended to analyze a typical two-spool multi-stage aeroengine rotor. Rotordynamic model is developed from sample geometric, material and bearing data. This is described in Chapter 4. Detailed parametric studies could not be carried out. Preliminary results on the free and residual unbalance response are presented.

CHAPTER 2

CRITICAL SPEEDS OF DUAL ROTORS

The first step in the dynamic analysis of any rotor-bearing system comprises of computation of critical speeds and mode shapes. Unbalance response analysis and consequent dynamic stress analysis is carried out after necessary critical speed calculation and free vibration analysis has been accomplished. In the present study, dual rotors are modeled through two separate procedures, namely - (i) transfer matrix method of Myklestad and Prohl (1944) and (ii) finite element technique, using standard available software. The modeling procedures and results are described in this chapter.

2.1 Transfer Matrix Method

The transfer matrix method, for far-coupled systems, suggested by Myklestad and Prohl has proved to be an effective tool for modeling rotor-bearing systems for bending vibration analysis. State vectors defined at various discrete stations along the rotor length are related through Field and Point matrices and boundary conditions are applied to obtain the frequency equation, which can be solved through any numerical technique.

2.1.1 Field Matrix

An n mass rotor system is shown in Fig 2.1(a). The rotor discs are located at stations 1, 2, ...n. The rotor is supported at stations 0 and n+1. The masses are taken to be lumped with gyroscopic inertia neglected. Defining the state vector at station i as

$$\{S\} = \begin{Bmatrix} -w \\ \theta \\ M_y \\ V_z \end{Bmatrix} \qquad (2.1)$$

where w is deflection; θ is the slope; M_y denotes the bending moment and V_z denotes shear force. The state vector can be defined to the left or rights of station i, as shown in Fig 2.1(b). l_i is the shaft element length and m_i is the mass located at the ith station in Fig 2.1(b). The relations across the ith field can be written as from Fig 2.2 (Rao, 1996)

$$-w_i^L = -w_{i-1}^R + \theta_{i-1}^R l_i + M_{y,i-1}^R \frac{l_i^2}{2EI_i} + V_{z,i-1}^R \frac{l_i^3}{3EI_i}$$

$$\theta_i^L = \theta_{i-1}^R + M_{y,i-1}^R \frac{l_i}{EI_i} + V_{z,i-1}^R \frac{l_i^2}{2EI_i} \tag{2.2}$$

$$M_{y,i}^L = M_{y,i-1}^L + V_{z,i}^L l_i$$

$$V_{z,i}^L = V_{z,i-1}^R$$

or in matrix form as

$$\begin{Bmatrix} -w \\ \theta \\ M_y \\ V_z \end{Bmatrix}_i^L = \begin{bmatrix} 1 & l & \frac{l^2}{2EI} & \frac{l^3}{6EI} \\ 0 & 1 & \frac{l}{EI} & \frac{l^2}{2EI} \\ 0 & 0 & 1 & l \\ 0 & 0 & 0 & 1 \end{bmatrix}_i \begin{Bmatrix} -w \\ \theta \\ M_y \\ V_z \end{Bmatrix}_{i-1}^R \tag{2.3}$$

Defining a Field Matrix

$$[F]_i = \begin{bmatrix} 1 & l & \frac{l^2}{2EI} & \frac{l^3}{6EI} \\ 0 & 1 & \frac{l}{EI} & \frac{l^2}{2EI} \\ 0 & 0 & 1 & l \\ 0 & 0 & 0 & 1 \end{bmatrix}_i \tag{2.4}$$

equation (2.3) can be symbolically written as

$$\{S\}_i^L = [F]_i \{S\}_{i-1}^R \tag{2.5}$$

2.1.2 Point Matrix

The force and moment balance relations across the ith mass (Fig 2.3) provide the following matrix equation

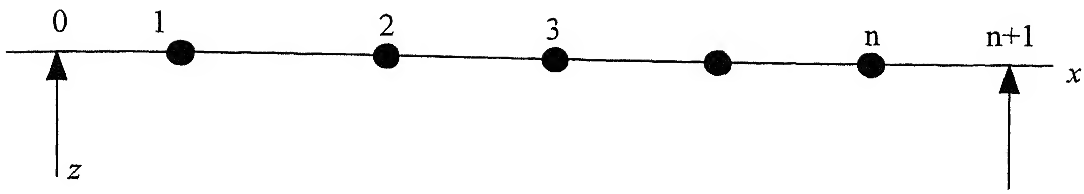

Figure 2.1(a) ***n* Mass rotor system**

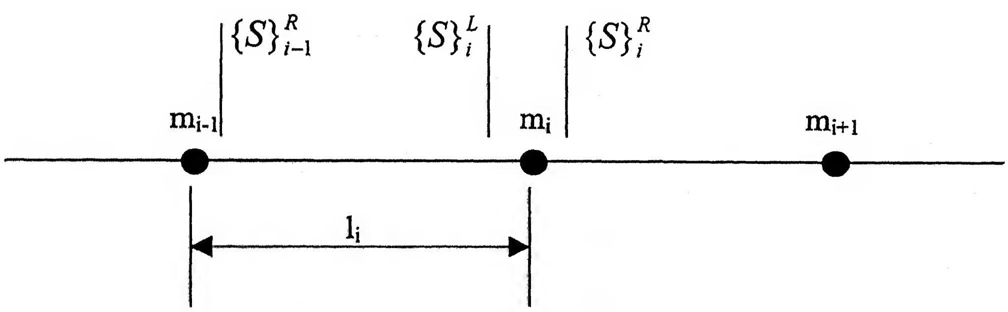

Figure 2.1(b) ***i*th Shaft element**

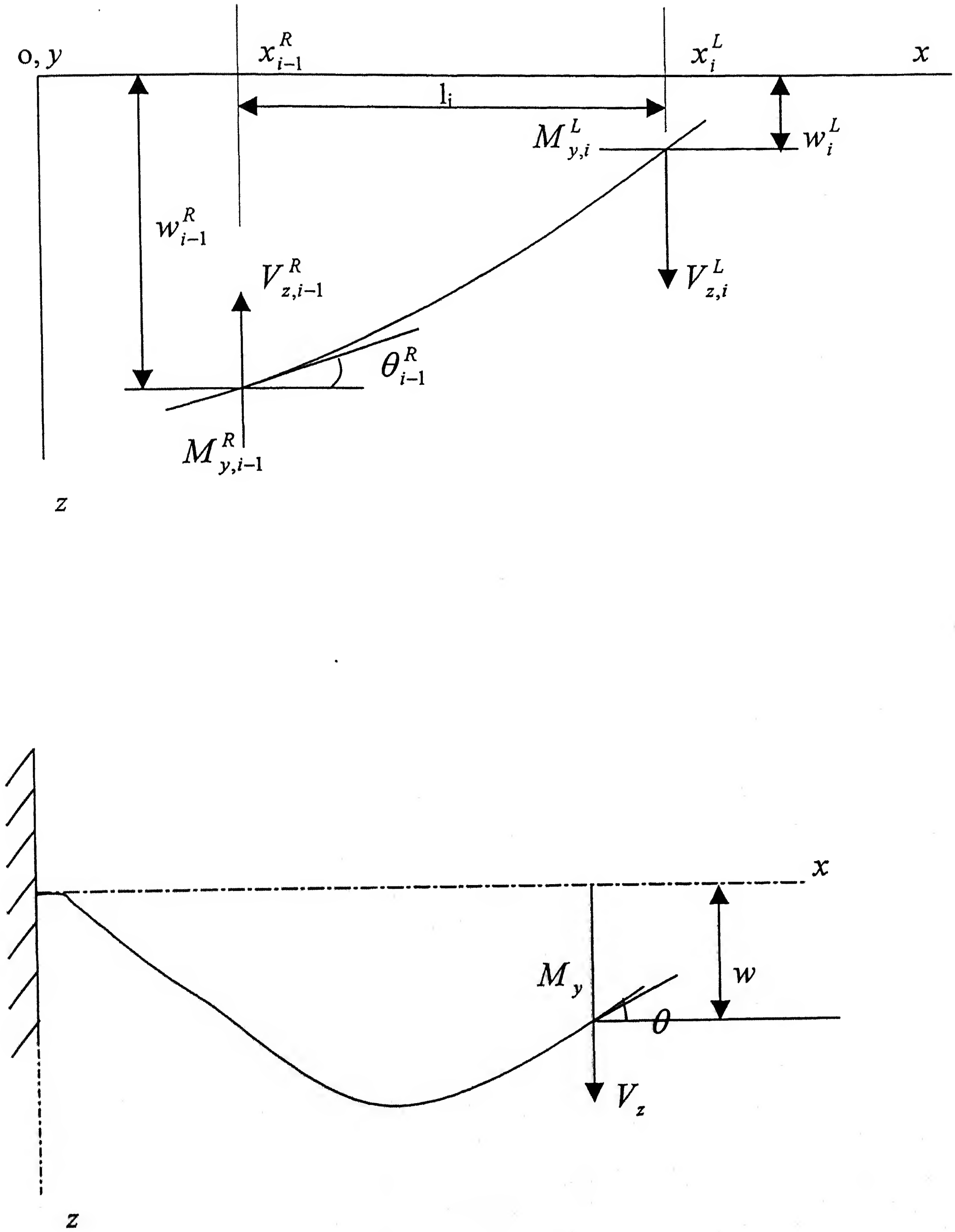

Figure 2.2 Relations for the i^{th} field

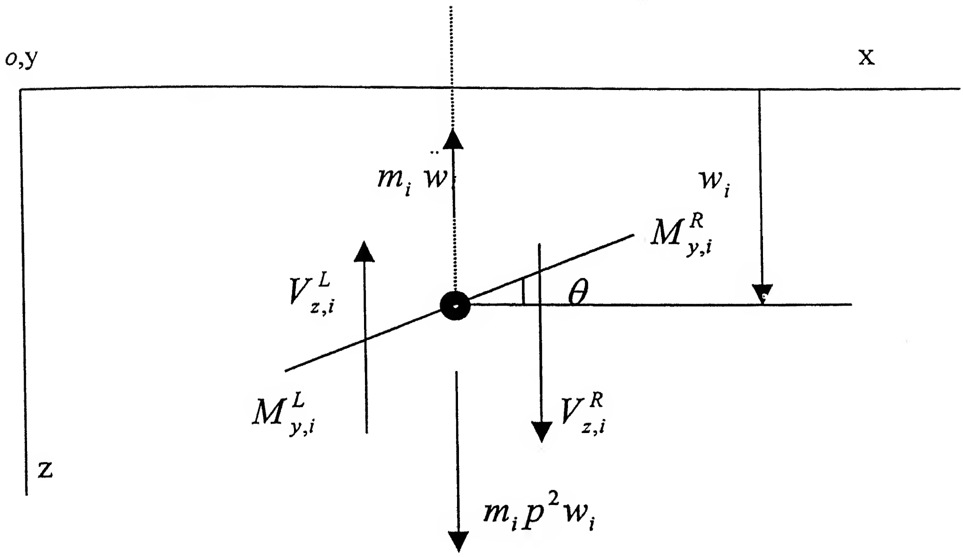

Figure 2.3 Equilibrium relations for the i[th] mass

$$\begin{Bmatrix} -w \\ \theta \\ M_y \\ V_z \end{Bmatrix}_i^R = \begin{bmatrix} 1 & 0 & 0 & 0 \\ 0 & 1 & 0 & 0 \\ 0 & 0 & 1 & 0 \\ mp^2 & 0 & 0 & 1 \end{bmatrix}_i \begin{Bmatrix} -w \\ \theta \\ M_y \\ V_z \end{Bmatrix}_i^L \tag{2.6}$$

Defining the ith Point Matrix as

$$[P]_i = \begin{bmatrix} 1 & 0 & 0 & 0 \\ 0 & 1 & 0 & 0 \\ 0 & 0 & 1 & 0 \\ mp^2 & 0 & 0 & 1 \end{bmatrix}_i \tag{2.7}$$

equation (2.6) can be symbolically expressed as

$$\{S\}_i^R = [P]_i\{S\}_i^L \tag{2.8}$$

2.1.3 Overall Transfer Matrix and Frequency Equation

Employing equations (2.5) and (2.8), the matrix relationship across stations 0 and n+1 can be written as

$$\begin{aligned}
&\{S\}_1^L = [F]_1\{S\}_0 \\
&\{S\}_1^R = [P]_1\{S\}_1^L = [P]_1[F]_1\{S\}_0 \\
&\{S\}_2^L = [F]_2\{S\}_1^R = [F]_2[P]_1[F]_1\{S\}_0 \\
&\cdots\cdots\cdots\cdots \\
&\{S\}_{n+1} = [F]_{n+1}[P]_n[F]_n[P]_{n-1}\cdots\cdots\cdots\cdots[F]_1\{S\}_0
\end{aligned} \tag{2.9}$$

Defining the product of all field and point matrices, in the order given in the above equation, as the overall transfer matrix $[U]$ one gets

$$\{S\}_{n+1} = [U]\{S\}_0 \tag{2.10}$$

Since field and point matrices are both of order 4, the overall transfer matrix is also 4x4 in size and equation (2.10) can be written in expanded form as

$$\begin{Bmatrix} -w \\ \theta \\ M_y \\ V_z \end{Bmatrix}_{n+1} = \begin{bmatrix} u_{11} & u_{12} & u_{13} & u_{14} \\ u_{21} & u_{22} & u_{23} & u_{24} \\ u_{31} & u_{32} & u_{33} & u_{34} \\ u_{41} & u_{42} & u_{43} & u_{44} \end{bmatrix} \begin{Bmatrix} -w \\ \theta \\ M_y \\ V_z \end{Bmatrix}_0 \tag{2.11}$$

Equation (2.11) is employed, after substitution of the boundary conditions appropriately, to obtain the frequency equation of the rotor and consequent computation of its critical speeds. For example, for a rotor supported in rigid bearings and modeled as a simply supported system, the boundary conditions are $w = 0$ and $M_y = 0$, at stations 0 and n+1, which upon substitution in equation (2.11) yield the following frequency equation

$$\begin{vmatrix} u_{12} & u_{14} \\ u_{32} & u_{34} \end{vmatrix} = 0 \tag{2.12}$$

An appropriate root searching technique can be employed to search for the values of critical speeds p_i in equation (2.12). Once the critical speed is determined, the corresponding mode shape is determined by assuming a unit slope at station 0, i.e., $\theta_0 = 1$ which gives $V_{z,0} = -u_{12}/u_{14}$ and thus the state vector at station 0 is completely defined. Employing the relations (2.5), (2.8) one can proceed to determine the state vectors at all stations and get the mode shape corresponding to the critical speed determined.

2.1.4 Gyroscopic Effects

Gyroscopic couple changes the bending moment equation across the mass, which is not considered earlier. The disks on the rotor contribute to the gyroscopic couple. For discs located at nodal points, the gyroscopic effect can be significant, especially in the case of overhang rotors, with a disk at the free end. Considering the spinning of the ith disk of the rotor, if the angular velocity is ω and the transverse and polar moment of inertia of the disk are I_T and I_P respectively, the precessional motion θ and ϕ in the x-z and x-y planes respectively, are governed by (refer Fig.2.4 a, b)

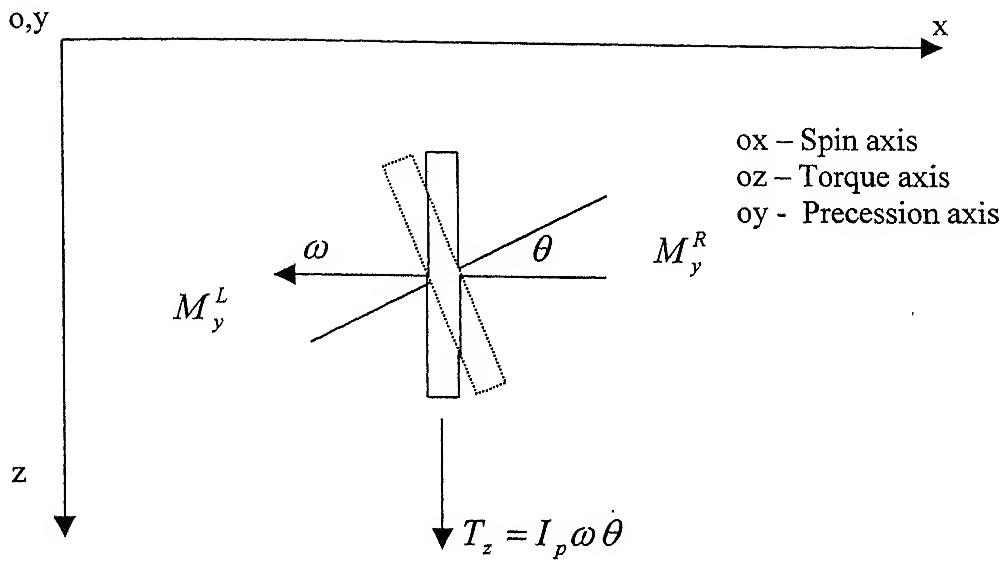

Figure 2.4(a) **Motion of spinning disk in *x-z* plane**

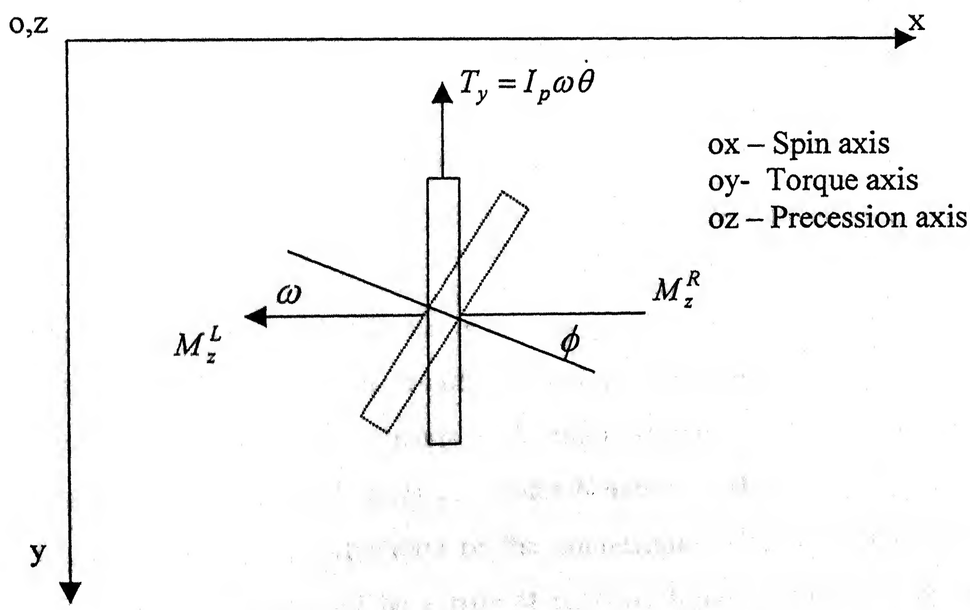

Figure 2.4(b) **Motion of spinning disk in *x-y* plane**

$$M_{yi}^{R} = M_{yi}^{L} + I_P \omega \dot{\phi}_i + I_T \ddot{\theta}_i$$

$$M_{zi}^{R} = M_{zi}^{L} - I_P \omega \dot{\theta}_i + I_T \ddot{\phi}_i \tag{2.13}$$

which modify the point matrix to

$$[P]_i = \begin{bmatrix} 1 & 0 & 0 & 0 \\ 0 & 1 & 0 & 0 \\ 0 & (I_P - I_T)(2\omega - p)p & 1 & 0 \\ m_i p^2 & 0 & 0 & 0 \end{bmatrix} \tag{2.14}$$

It is to be noted that forward synchronous whirl of the rotor would correspond to the case $\omega = p$, while backward synchronous whirl corresponds to $\omega = -p$. The effect of gyroscopic couple is to stiffen the rotor and raise the critical speed. Due to gyroscopic effect the natural frequency of rotor system changes with rotating speed.

2.1.5 Intershaft Coupling

The transfer matrix procedure employing point and field matrices described above with appropriate modifications for gyroscopic effects is an efficient tool for finding the natural frequencies of single-shaft / spool rotor system. However, in case of multi-shaft / spool rotor system the dynamic behavior of one rotor is affected by another due to the presence of intershaft bearings and this makes its mathematical analysis different.

Figure 2.5 shows the scheme of a typical multi-spool rotor system with several intershaft bearings. It consists of *N* rotors and *M* intershaft bearings. The system is divided into *N+M* subsystems - *N* rotor systems and *M* inter shaft bearings subsystems, i.e., rotor 1, rotor 2, ...rotor *N* and inter-shaft bearings with impedances Z_{b1}, Z_{b2} ... Z_{bm}. On separation of the connections of every intershaft bearing, the constraint condition will be a pair of external force vectors R_{yj}, R_{zj} added on the connecting point *j*, in the *y* and *z* directions respectively. The transfer matrix method is now employed for the rotor sub-systems. For subsystem rotor *i*, the boundary condition will be

$$M^i_{yo} = M^i_{z0} = 0,$$
$$M^i_{yk} = M^i_{zk} = 0, \tag{2.15}$$

$$V^i_{y0} = V^i_{z0} = 0$$
$$V^i_{yk} = V^i_{zk} = 0 \tag{2.16}$$

The relationship between the state variables on section 0 and the left side of station 1 in ith rotor will be

$$\{S\}_1^{iL} = [U]_1^i \{S\}_0^i \tag{2.17}$$

The state vector on the right side of station 1 will be

$$\{S\}_1^{iR} = \left\{-w, \theta, M_y, V_z + R_z, v, \phi, M_z, -V_y + R_y\right\}_1^{iT} \tag{2.18}$$

The relationship between the state vector on the sections of the right side of station 1 and left side of station 2 will be

$$\{S\}_2^{iL} = [U]_2^i \{S\}_1^{iR} \tag{2.19}$$

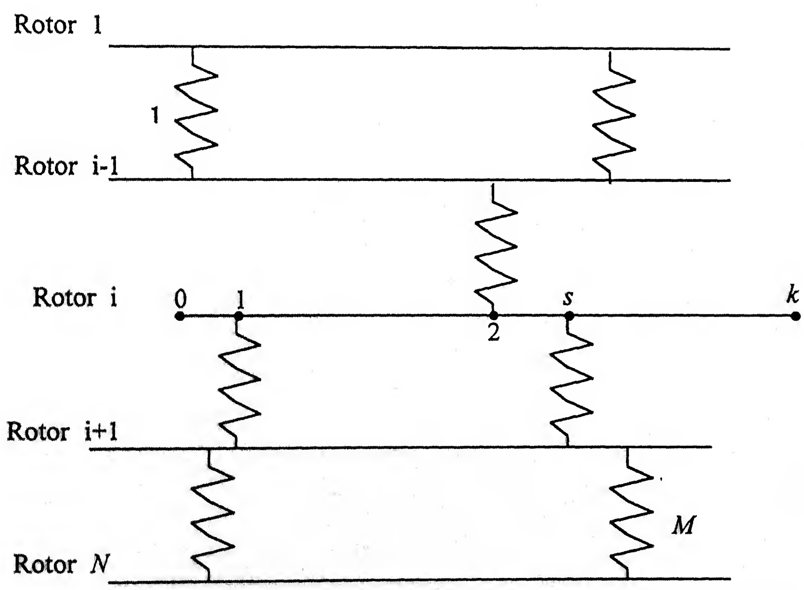

Figure 2.5 **General multi-spool rotor system scheme**

Similarly, the state vector on the section of the right side of station 2 will be:

$$\{S\}_2^{iR} = \left\{-w, \theta, M_y, V_z + R_z, v, \phi, M_z, -V_y + R_y\right\}_2^{iT} \tag{2.20}$$

The relationship between the state vector on section of the left and right sides of the segments, s-k, will be:

$$\{S\}_k^i = [U]_k^i \{S\}_s^{iR} \tag{2.21}$$

where

$$\{S\}_s^{iR} = \left\{-w, \theta, M_y, V_z + R_z, v, \phi, M_z, -V_y + R_y\right\}_s^{iT} \tag{2.22}$$

According to the boundary conditions (2.15, 2.16), the following equations can be obtained:

$$\left.\begin{aligned} M_{yk}^i &= \sum_{j=1}^{8} U_k^i(3,j)\{S\}_{sR}^i(j) = 0 \\ V_{zk}^i &= \sum_{j=1}^{8} U_k^i(4,j)\{S\}_{sR}^i(j) = 0 \end{aligned}\right. \tag{2.23}$$

$$\left.\begin{aligned} M_{zk}^i &= \sum_{j=1}^{8} U_k^i(7,j)\{S\}_{sR}^i(j) = 0 \\ V_{yk}^i &= \sum_{j=1}^{8} U_k^i(8,j)\{S\}_{sR}^i(j) = 0 \end{aligned}\right. \tag{2.24}$$

Substituting equations (2.17)-(2.22) in to equation (2.23) and (2.24), the following four homogeneous ordinary equations will be obtained

$$\begin{aligned} &A(4i-3,4i-3)w_0^i + A(4i-3,4i-2)\theta_0^i + A(4i-3,4i-1)v_0^i + A(4i-3,4i)\phi_0^i \\ &+ A(4i-3,4N+1)R_{y1} + \ldots\ldots + A(4i-3,4N+s)R_{ys} + A(4i-3,4N+s+1)R_{z1} \\ &+ \ldots\ldots\ldots + A(4i-3,4N+2s)R_{zs} = 0 \end{aligned}$$

$$\begin{aligned} &A(4i-2,4i-3)w_0^i + A(4i-2,4i-2)\theta_0^i + A(4i-2,4i-1)v_0^i + A(4i-2,4i)\phi_0^i \\ &+ A(4i-2,4N+1)R_{y1} + \ldots\ldots + A(4i-2,4N+s)R_{ys} + A(4i-2,4N+s+1)R_{z1} \\ &+ \ldots\ldots\ldots + A(4i-2,4N+2s)R_{zs} = 0 \end{aligned}$$

$$\begin{aligned} &A(4i-1,4i-3)w_0^i + A(4i-1,4i-2)\theta_0^i + A(4i-1,4i-1)v_0^i + A(4i-1,4i)\phi_0^i \\ &+ A(4i-1,4N+1)R_{y1} + \ldots\ldots + A(4i-1,4N+s)R_{ys} + A(4i-1,4N+s+1)R_{z1} \\ &+ \ldots\ldots\ldots + A(4i-1,4N+2s)R_{zs} = 0 \end{aligned}$$

$$A(4i,4i-3)w_0^i + A(4i,4i-2)\theta_0^i + A(4i,4i-1)v_0^i + A(4i,4i)\phi_0^i + A(4i,4N+1)R_{y1} + \ldots\ldots + A(4i,4N+s)R_{ys} + A(4i,4N+s+1)R_{z1} + \ldots\ldots\ldots + A(4i-3,4N+2s)R_{zs} = 0 \qquad (2.25)$$

where $A(i,j)$ is a function of the concerned transfer matrices $[U]_1^i,[U]_2^i\ldots\ldots[U]_k^i$. For N rotor subsystem, $4N$ equations are obtained. There are, however, $4N+2M$ unknown state variables $w_0^1,\theta_0^1,v_0^1,\phi_0^1,\ldots\ldots w_0^N,\theta_0^N,v_0^N,\phi_0^N,R_{y1},\ldots R_{yM},R_{z1}\ldots\ldots R_{zM}$. The $2M$ supplemental equations for searching for all these variables can be obtained by impedance matching at the connecting points. Considering an intershaft bearing connecting two-rotor subsystem, as shown in Fig 2.6, the following equation must be satisfied

$$\begin{Bmatrix} R_{zj} \\ R_{yj} \end{Bmatrix} = Z_{bj} \begin{Bmatrix} w_j^i - w_j^{i+1} \\ v_j^i - v_j^{i+1} \end{Bmatrix} \qquad (2.26)$$

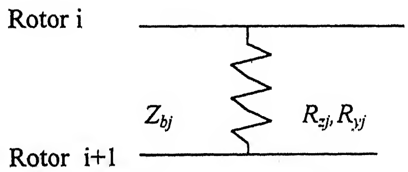

Figure 2.6 Bearing Impedance

Deflections $w_j^i,v_j^i,w_j^{i+1},v_j^{i+1}$, in equation (2.26), can be expressed as the functions of $w_0^i,\theta_0^i,\ldots\ldots v_0^{i+1},\varphi_o^{i+1}$ and the concerned transfer matrices $[U]_1^i\ldots\ldots[U]_j^i$ and $[U]_1^{i+1}\ldots\ldots[U]_j^{i+1}$, so that, equation (2.26) can be written as the following set of equations

$$A(4N+j,4i-3)w_0^i + A(4N+j,4i-2)\theta_0^i + A(4N+j,4i-1)v_0^i + A(4N+j,4i)\phi_0^i + A(4N+j,4i+1)w_0^{i+1} + A(4N+j,4i+2)\theta_0^{i+1} + A(4N+j,4i+3)v_0^{i+1} + A(4N+j,4i+4)\phi_0^{i+1} + A(4N+j,4N+1)R_{x1} + \ldots\ldots + A(4N+j,4N+j)R_{xj} + A(4N+j,4N+M+1)R_{y1} + \ldots\ldots\ldots\ldots\ldots\ldots + A(4N+j,4N+M+j)R_{yj} = 0 \qquad (2.27)$$

$$A(4N+M+j,4i-3)w_0^i + A(4N+M+j,4i-2)\theta_0^i + A(4N+M+j,4i-1)v_0^i +$$
$$A(4N+M+j,4i)\phi_0^i + A(4N+M+j,4i+1)w_0^{i+1} + A(4N+M+j,4i+2)\theta_0^{i+1} +$$
$$A(4N+M+j,4i+3)v_0^{i+1} + A(4N+M+j,4i+4)\phi_0^{i+1} + A(4N+M+j,4N+1)R_{x1}$$
$$+ \dots\dots + A(4N+M+j,4N+j)R_{xj} + A(4N+M+j,4N+M+1)R_{y1} + \dots\dots +$$
$$A(4N+M+j,4N+M+j)R_{yj} = 0 \qquad (2.28)$$

For M intershaft bearings, $2M$ homogeneous equations can be obtained. Now a set of homogeneous ordinary equations will consist of $4N+2M$ equations according to equations (2.25), (2.27) and (2.28) and can be represented in matrix form as

$$[A]\{S\} = 0 \qquad (2.29)$$

where

$$\{S\} = \{w_0^1, \theta_0^1, v_0^i, \phi_0^1, \dots\dots w_0^N, \theta_0^N, v_0^N, \phi_0^N, R_{x1}, \dots\dots R_{xM}, R_{y1}, \dots\dots R_{yM}\}^T \qquad (2.30)$$

Equation (2.29) can be solved through an appropriate routine to obtain eigenvalues and eigenvectors.

2.1.5 Case Study 1

The application of the transfer matrix method, described above, is illustrated through the following example. An undamped dual rotor containing two isotropic intershaft bearings, as shown in Fig.2.7 is considered. Each shaft carries two discs. An exact solution of this problem has been obtained by Taipeng (1988). He also employed the method of component mode synthesis and compared the results with the exact solution.

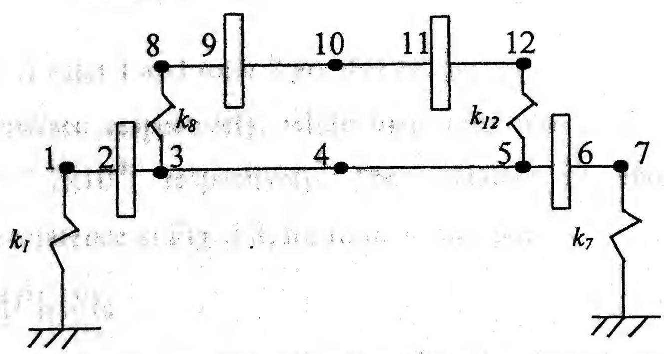

Fig. 2.7 Dual rotor system - Case Study 1

The division into subsystems - rotor 1, rotor 2 and intershaft bearings k_8 and k_{12} is shown in Fig.2.8

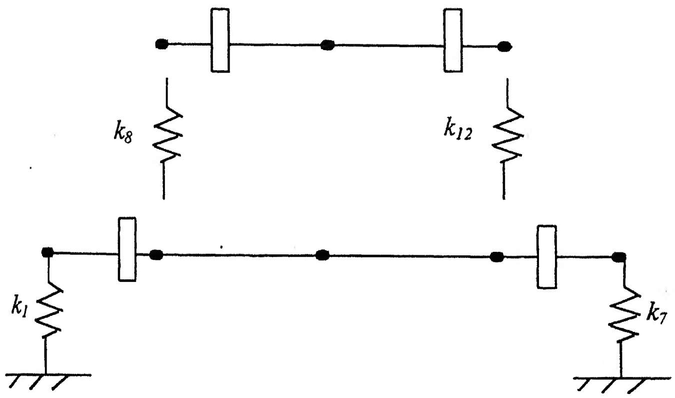

Figure-2.8 Sub-systems of the dual rotor - Case Study 1

Table 2.1 Dual rotor system data -Case Study 1

Station No.	Mass (Kg)	I_p (Kg-m^2)	K (N/m)	l (m)
1	00.325	0.0	2.5×10^7	0.075
2	10.450	0.113	-	0.075
3	00.935	0.0	-	0.225
4	01.321	0.0	-	0.225
5	00.925	0.0	-	0.075
6	08.450	0.090	-	0.075
7	00.305	0.0	1.5×10^7	
8	00.193	0.0	1.2×10^7	
9	07.780	0.071	-	0.075
10	00.373	0.0	-	0.150
11	06.280	0.043	-	0.150
12	00.173	0.0	1.0×10^7	0.075

The rotational speeds of rotor 1 and rotor 2 are 994.88 rad/sec and axis of rotor 1 and rotor 2 are 994.88 rad/sec respectively, while their area moments of inertia are 3.976×10^{-8} m^4 and 5.2×10^{-8}, respectively. The modulus of elasticity, E is 2.07×10^{11}N/m^2. With reference to Fig. 2.8, for roror 1, one gets

$$\{S\}_3^L = [F]_2[P]_2[F]_1[\bar{P}]_1\{S\}_0 \qquad (2.31)$$

where, $\{S\}_0$ is the state vector to the left of station 1. Continuing further, the following matrix relations can be obtained

$$\{S\}_3^R = [P]_3\{S\}_3^L + \{R_1\}$$

$$\{S\}_5^L = [F]_4[P]_4[F]_3\{S\}_3^R$$

$$\{S\}_5^R = [P]_5\{S\}_5^L + \{R_2\}$$

$$\{S\}_7^R = [\overline{P}]_7[F]_6[P]_6[F]_5\{S\}_5^R$$

$$\{S\}_7^R = [\overline{P}]_7[F]_6[P]_6[F]_5[[P]_5\{S\}_5^L + \{R_2\}]$$

$$\{S\}_7^R = [\overline{P}]_7[F]_6[P]_6[F]_5[[P]_5[F]_4[P]_4[F]_3\{S\}_3^R + \{R_2\}]$$

$$\{S\}_7^R = [\overline{P}]_7[F]_6[P]_6[F]_5[[P]_5[F]_4[P]_4[F]_3[[P]_3\{S\}_3^L + \{R_1\}] + \{R_2\}] \qquad (2.32)$$

$[\overline{P}]_1$ and $[\overline{P}]_7$ are modified point matrix to include the effect of spring stiffness.

Similarly, for rotor-2, one gets

$$\{S\}_8^R = [P]_8\{S\}_8^L - \{R_1\}$$

$$\{S\}_{12}^L = [F]_{11}[P]_{11}[F]_{10}[P]_{10}[F]_9[P]_9[F]_8\{S\}_8^R$$

$$\{S\}_{12}^R = [P]_{12}\{S\}_{12}^L - \{R_2\}$$

$$\{S\}_{12}^R = [P]_{12}[F]_{11}[P]_{11}[F]_{10}[P]_{10}[F]_9[P]_9[F]_8\{S\}_8^R - \{R_2\}$$

$$\{S\}_{12}^R = [P]_{12}[F]_{11}[P]_{11}[F]_{10}[P]_{10}[F]_9[P]_9[F]_8[[P]_8\{S\}_8^L - \{R_1\}] - \{R_2\} \qquad (2.33)$$

The bearing reaction vectors are

$$\begin{aligned} \{R_1\} &= \{0 \;\; 0 \;\; 0 \;\; -k_8(w_3^L - w_8^L)\}^T \\ \{R_2\} &= \{0 \;\; 0 \;\; 0 \;\; -k_{12}(w_5^L - w_{12}^L)\}^T \end{aligned} \qquad (2.34)$$

Employing equations (2.34) and the following boundary conditions in equations (2.32) and (2.33),

$$\begin{aligned} M_{y1} &= M_{y7} = M_{y8} = M_{y12} = 0 \\ V_{z1} &= V_{z7} = V_{z8} = V_{z12} = 0 \end{aligned} \qquad (2.35)$$

the eigenvalue problem of equation (2.29) can be set up.

The algorithm for solving the eigenvalue problem has been written in MATLAB to compute the natural frequencies and mode shapes. The results obtained are given in

Table 2.1 along with those obtained by Taipeng (1988) from the exact solution. The difference between the natural frequencies is less than 0.01%, which serves to validate the transfer matrix procedure and MATLAB algorithm.

Table 2.2 Natural frequencies of the dual rotor system (Case Study 1)

Mode *	Exact (Rad/Sec)	Program (Rad/sec)
B	174.716	174.72
F	400.436	400.45
B	518.674	518.68
B	632.988	632.99
F	894.410	894.42
B	1349.958	1350.00
B	1397.403	1397.40
F	1432.092	1432.10
B	1805.751	1805.80
F	1829.741	1829.80
B	1868.237	1868.20
F	2119.298	2119.30
B	2292.203	2292.20
B	2637.412	2637.40
F	3056.654	3056.70
F	3422.186	3422.20
F	3721.947	3722.00
F	4752.938	4752.90

* B-Backward Whirl; F-Forward Whirl

2.2 Finite Element Model

Modeling of multi-spool rotors was carried out using the general-purpose finite element software NISA v-7.0. This software is being used in a cost-effective manner in a number of rotordynamic applications. However, its limitations, while modeling a dual rotor, with shafts rotating at different speeds, became evident during the course of this study. The steps to be followed while modeling a rotor in NISA are briefly described here.

NISA employs DISPLAY-III as a pre and post processor, and NISA-ADVANCED DYNAMICS to calculate the eigenvalues and vectors of rotor system. Modeling

process in NISA can be divided in two broad steps - Geometric Modeling and Finite Element Modeling.

2.2.1 Geometric modeling

The geometry of the dual rotor, in the present study, has been represented by employing a solid primitive cylinder and hyperpatch. For geometric modeling macro provision of NISA is used. It is a set of statements (program) which can be executed in DISPLAY III to model geometry in terms of variables and thereby can be used to create parametric models by inserting different values for the variable.

2.2.2 Finite Element modeling

3D solid hexahedral elements (Fig. 2.9) - NKTP = 4, DOF = 3 (UX, UY, UZ) are used to model the dual rotor . The discs are also modeled using 3D solid hexahedral elements. 3D translational spring elements (NKTP=17,DOF=3 UX, UY, UZ) are used to model intershaft and end bearings. All required geometric and material properties are defined through the NISA II 'forms' structure.

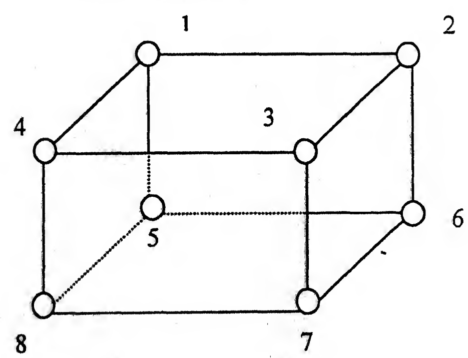

Figure 2.9 Hexahedral element with Nodes 1 to 8

2.2.3 Case Study 2

The modeling in NISA and computation of natural frequencies and mode shapes is illustrated through the example of the dual rotor chosen by Rajan, Nelson and Chen (1986). The rotor has also been analyzed through the transfer matrix method described in earlier sections, for verification of mode shapes. The rotor is shown in Figs. 2.10 (a), (b) and the physical and geometric data are given in Table 2.3 (a)-(c).

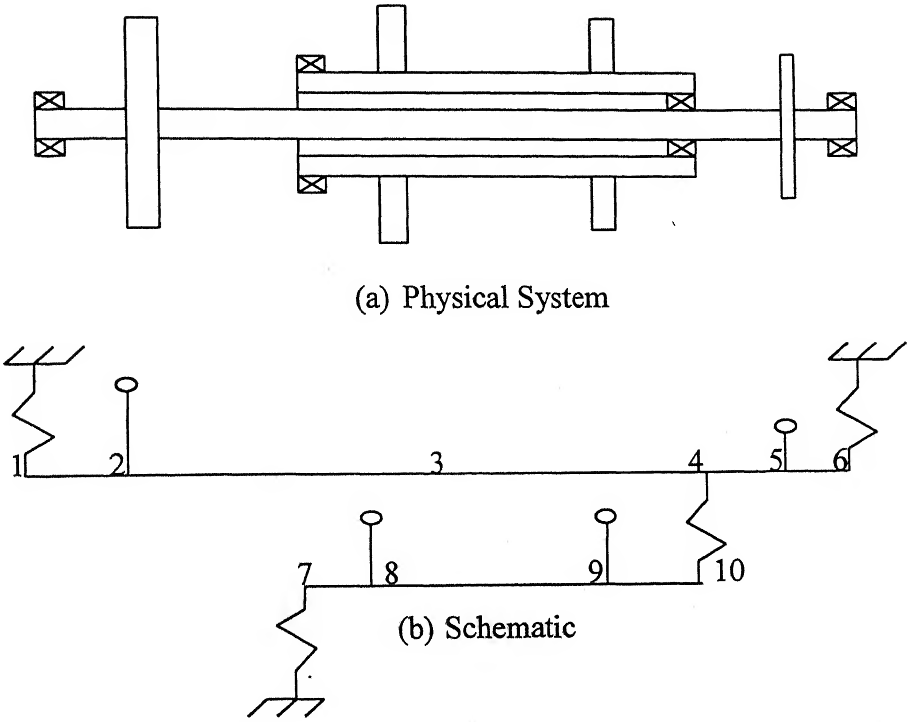

(a) Physical System

(b) Schematic

Figure 2.10 Dual rotor

Table 2.3 (a) Rotor Subelement Data (Case Study 2)

Shaft No.	**Element No.**	**Subelement No.**	**Length** (10^{-2}) m	**Inner Radius** (10^{-2}) m	**Outer Radius** (10^{-2}) m
1	1	1	7.62	0.	1.524
	2	1	8.89	0.	1.524
	2	2	8.89	0.	1.524
	3	1	7.62	0.	1.524
	3	2	762	0.	1.524
	4	1	5.08	0.	1.524
	5	1	5.08	0.	1.524
2	7	1	5.08	1.905	2.54
	8	1	7.62	1.905	2.54
	8	2	7.62	1.905	2.54
	9	1	5.08	1.905	2.54

$E = 206.9\text{x}10^9$ N/m^2 $\rho = 8304$ Kg/m^3

Table 2.3 (b) **Rotor Concentrated Disk Data (Case Study 2)**

Shaft No.	Station No.	Mass (Kg)	Polar Inertia ($kg\text{-}cm^2$)	Diametral Inertia ($kg\text{-}cm^2$)
1	2	4.904	271.2	135.6
	5	4.203	203.4	101.7
2	8	3.327	146.9	073.4
	9	2.277	097.2	048.6

Table2.3 (c) Rotor Bearing Data (Case Study 2)

Shaft No.	Station (a)	Station (b)	Stiffness (N/cm)
1	1	0	262,795
	4	10	087,598
	6	0	175,197
2	7	0	175,197

(0 denotes a connection to the rigid base)

The NISA model of the rotor, along with the co-ordinate system used are shown in Figs. 2.10 (a), (b). It needs to be mentioned that simulation of the shaft-disk assembly needs the additional procedure of simulating the interference fit between them. This is done by making the nodes, on the inner periphery the hole of the disc, lie on their counterparts of the shaft's outer periphery. The nodes are then merged with specified tolerance. The tolerance decides the type of fit, which is required to be obtained in the assembly. Close nodal merging tolerance of 0.001mm were ensured during assembly in order to simulate the interference fit condition of real life rotor system. A major limitation posed by NISA software is that it does not provide for rotation of components. Effects like gyroscopic couples can be simulated only through specific application of torque, which needs to be computed separately, for every component and rotating speed. During the present study, free vibration solution in NISA, does not incorporate gyroscopic influences. The NISA solution however provides good estimates of the natural frequencies, since gyroscopic couples are higher order effects. The mode shape approximation is also good and provides with three-dimensional facilities for motion visualization. The natural frequencies of the rotor obtained through this FEM model along with those from Rajan, Nelson and Chen (1986) and the transfer matrix method are given in Table 2.4.

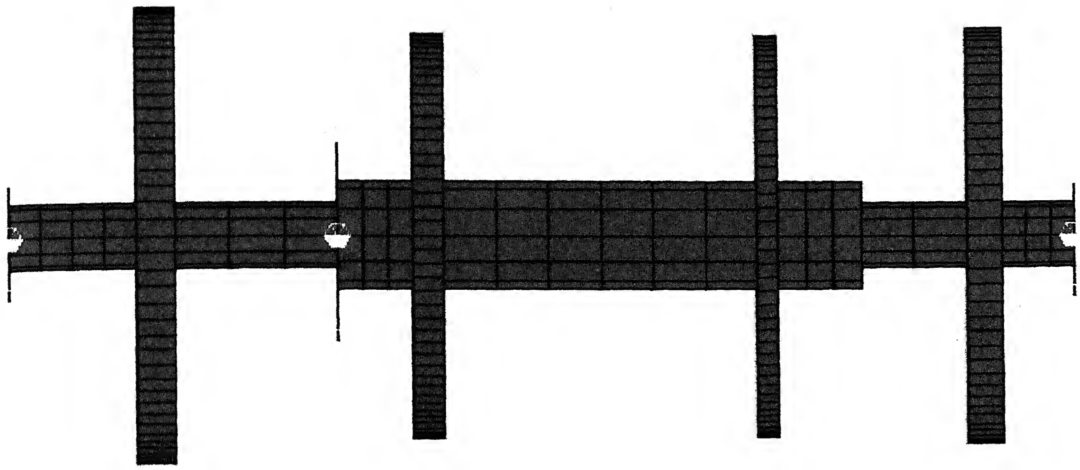

Figure 2.11(a) The Finite Element model of Dual Rotor

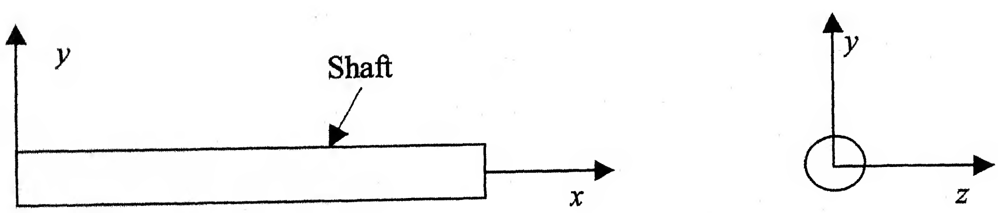

Figure 2.11(b) Coordinate system for 3D FE model

Table 2.4 Natural Frequencies (rad/s.) of Dual Rotor (Case Study 2)

Rajan et al (1986)	T M Method	FEM (NISA) (Solid Element)	(FEM) NISA (Beam Element)
755.0	771.0	755.9	749.42
1531.0	1593.0	1445.5	1540.92
2244.0	2220.0	1949.5	2261.40

It can be observed that the beam element model in FEM gives natural frequency values, which are closer to the Transfer Matrix model of the present study and that of Rajan et al, since the beam element simulates similar degrees of freedom as those in the Transfer Matrix models. Solid element model however provides the advantage of visualization of stress distribution, resultant displacements and contour plots. The first three mode shapes of the rotor corresponding to transverse vibration are given in Figs. 2.12 and 2.13. Figs. 2.12 correspond to the beam element model, while Figs.2.13 pertain to the solid element model. The mode shapes from the two models can be seen to be similar. The degree of flexure in the outer rotor in all three cases appears to significantly less than that of the inner rotor on which it is supported through the intershaft bearings. In the second mode, the nodal point for the inner rotor is close intershaft bearing number 2 (on the right), while in mode 3 the nodal point has shifted towards intershaft bearing number 1. This is also reflected in the contour plots, which show maximum stress at the junction points of the two rotors.

The critical speeds of this rotor, for forward and backward synchronous whirl with inner and outer rotor, and the corresponding mode shapes have been obtained by using transfer matrix method. These results are listed in Table 2.5 (a), (b).

Table2.5 (a) Critical Speeds (rad/s) - Synchronous whirl with inner rotor (Case Study 2)

Forward Whirl		Backward whirl	
Rajan et al (1986)	Present Study T.M.M.	Rajan et al (1986)	Present Study T.M.M.
863	895	660	676
1606	1692	1423	1458
2283	2269	2125	2090

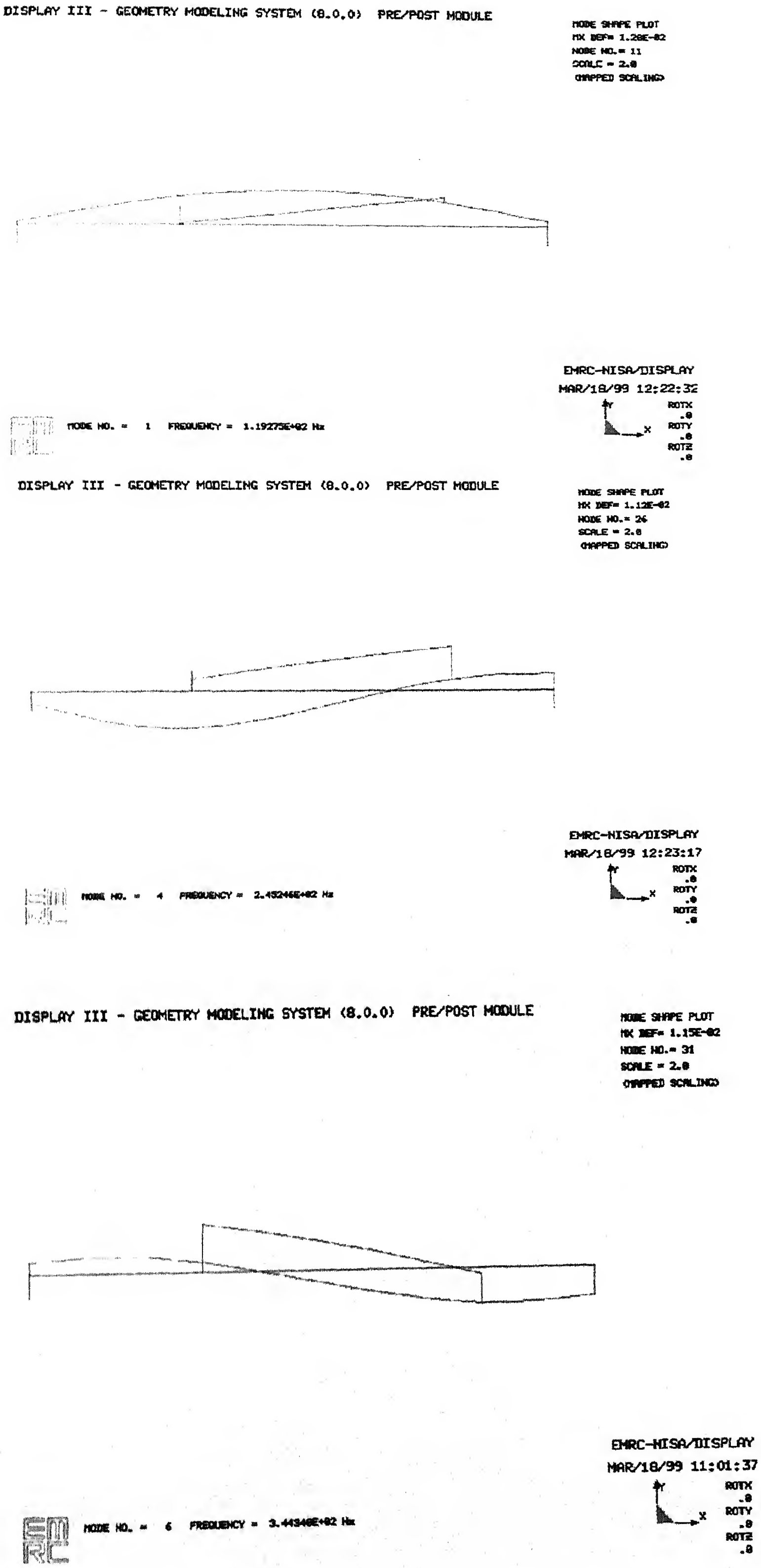

Figure 2.12 Modeshapes (case study 2) - beam element model

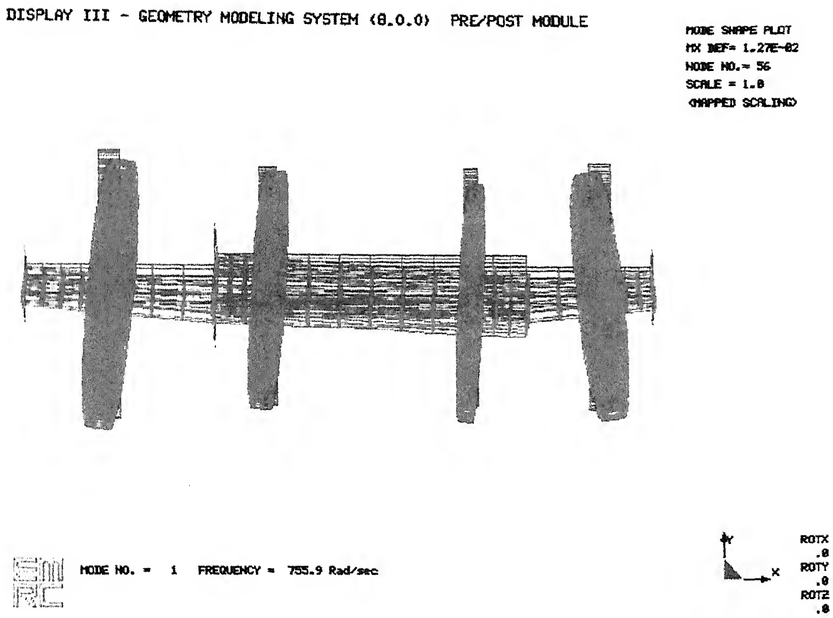

(I)

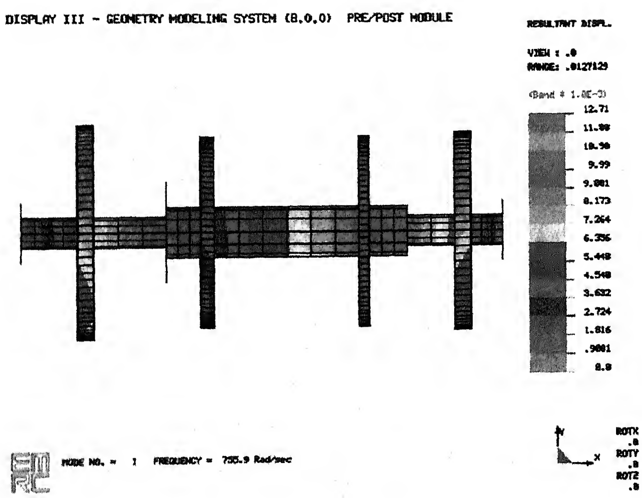

(II)

Figure 2.13(a) **I Mode (Case Study 2)-Solid Element**
(I) Mode Shape
(II) Contour Plot

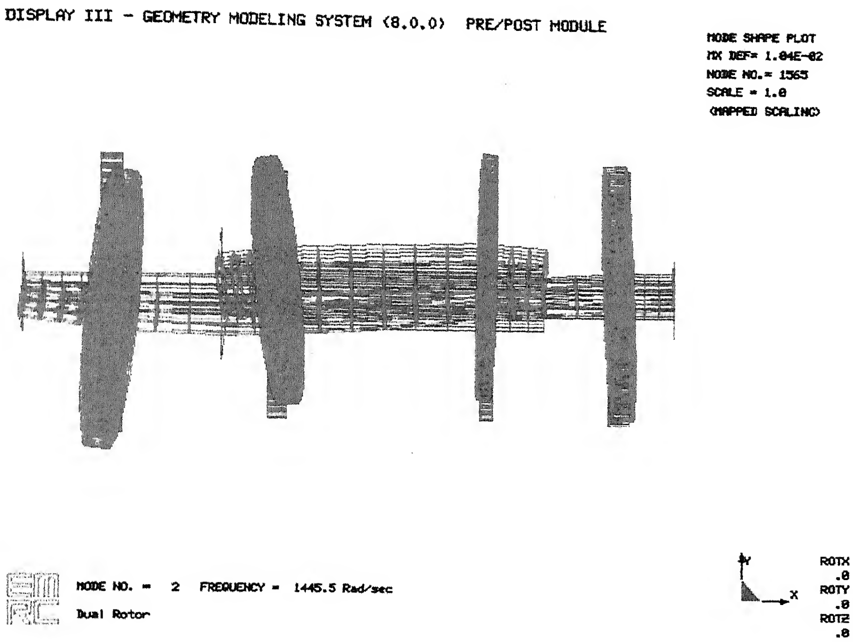

(I)

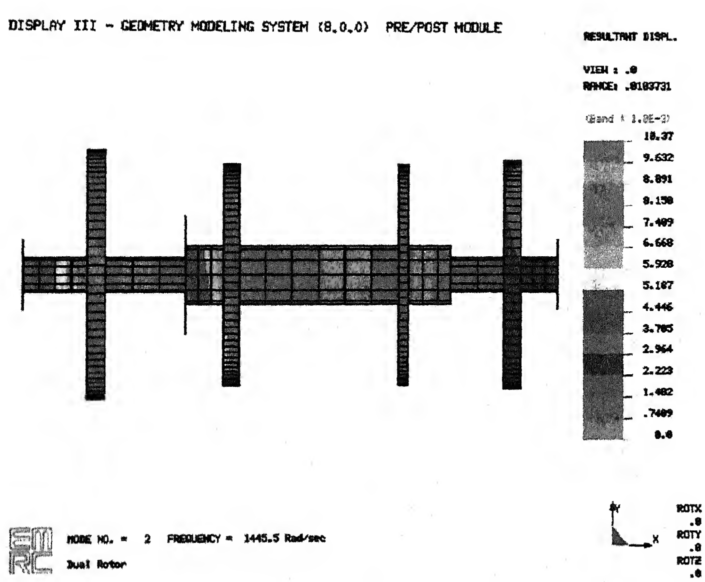

(II)

Figure 2.13(b) **II Mode (Case Study 2)-Solid Element**
(I) Mode Shape
(II) Contour Plot

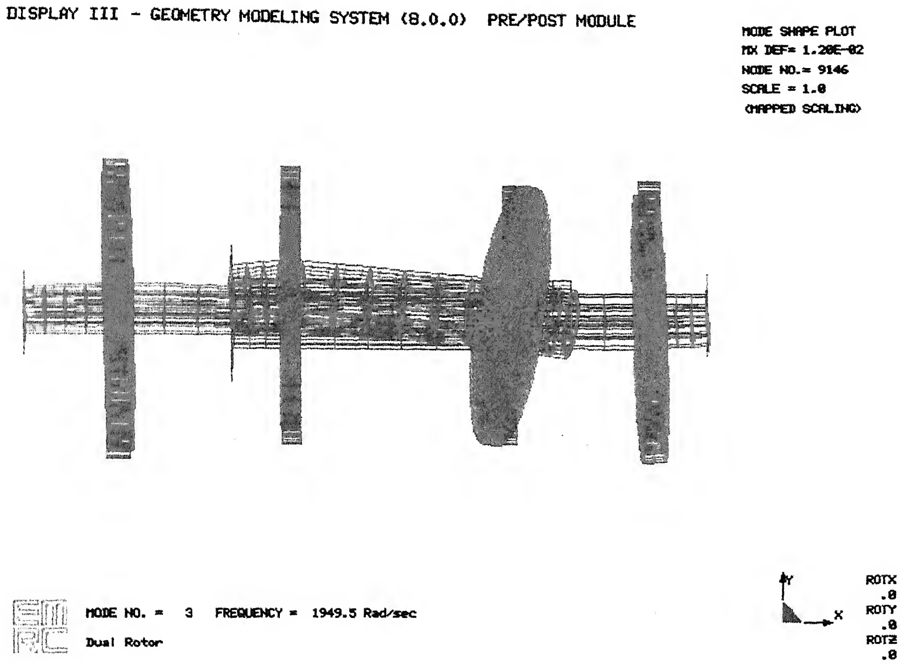

(I)

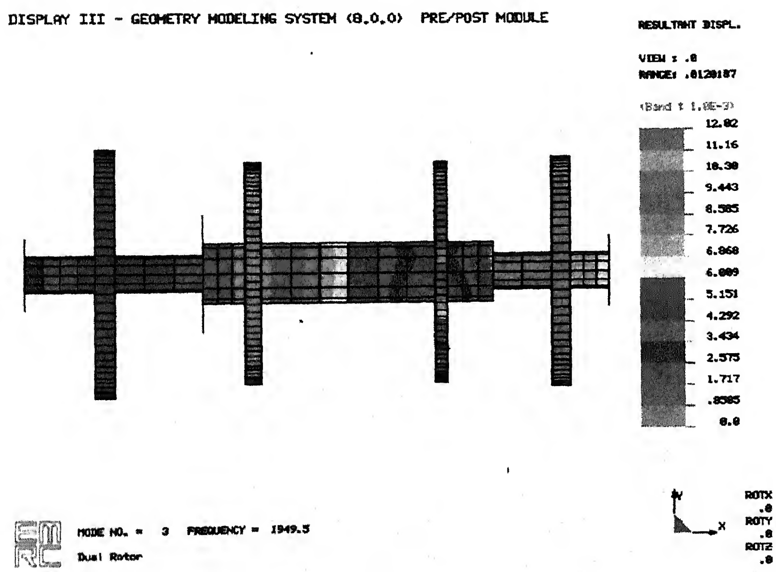

(II)

Figure 2.13(c) **III Mode (Case Study 2)-Solid Element**
(I) Mode Shape
(II) Contour Plot

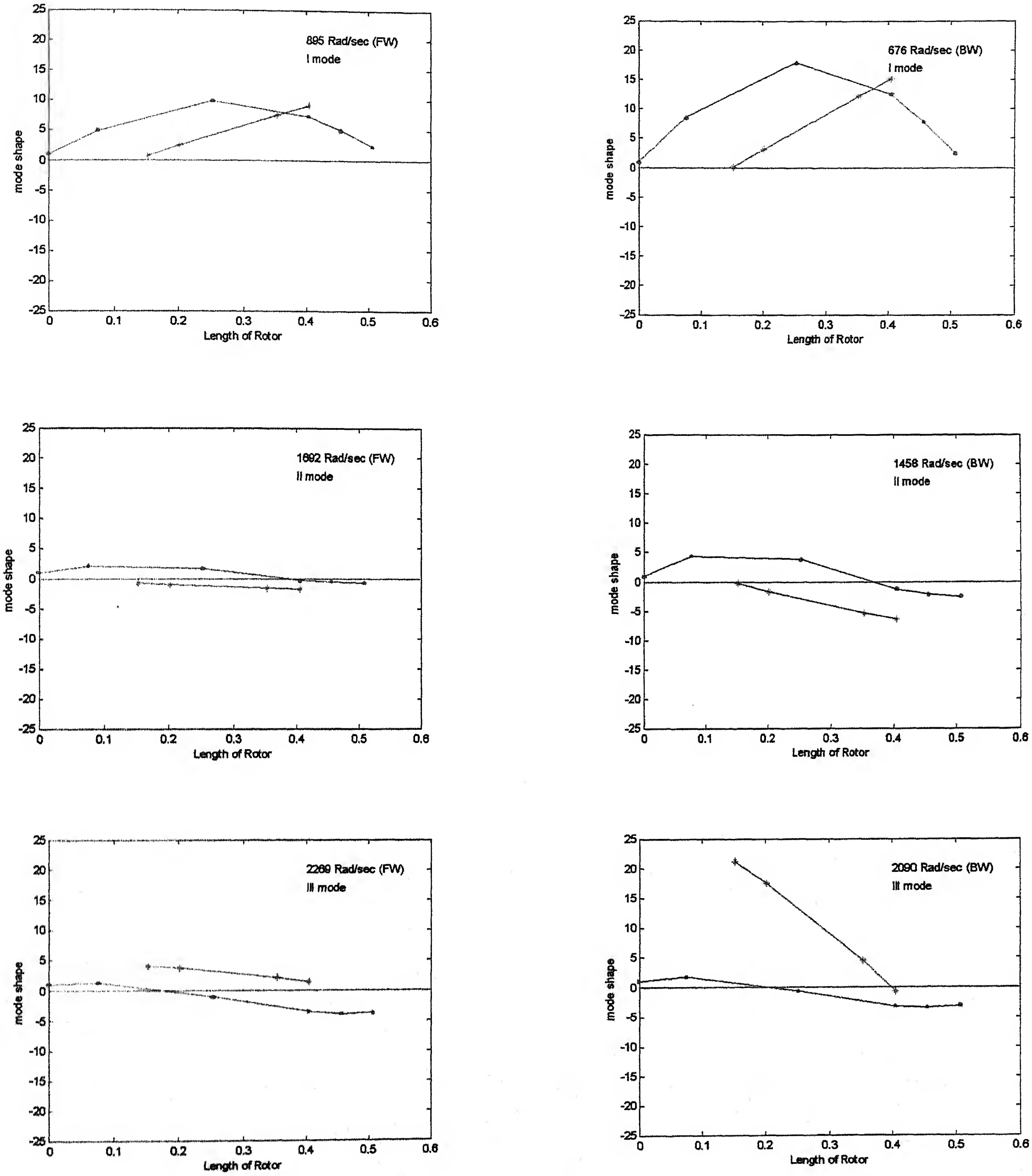

FW = Forward Whirl

BW = Backward Whirl

Figure 2.14(a) **Mode shapes corresponding to critical speeds (Case Study 2) (Synchronous whirl with inner rotor)**

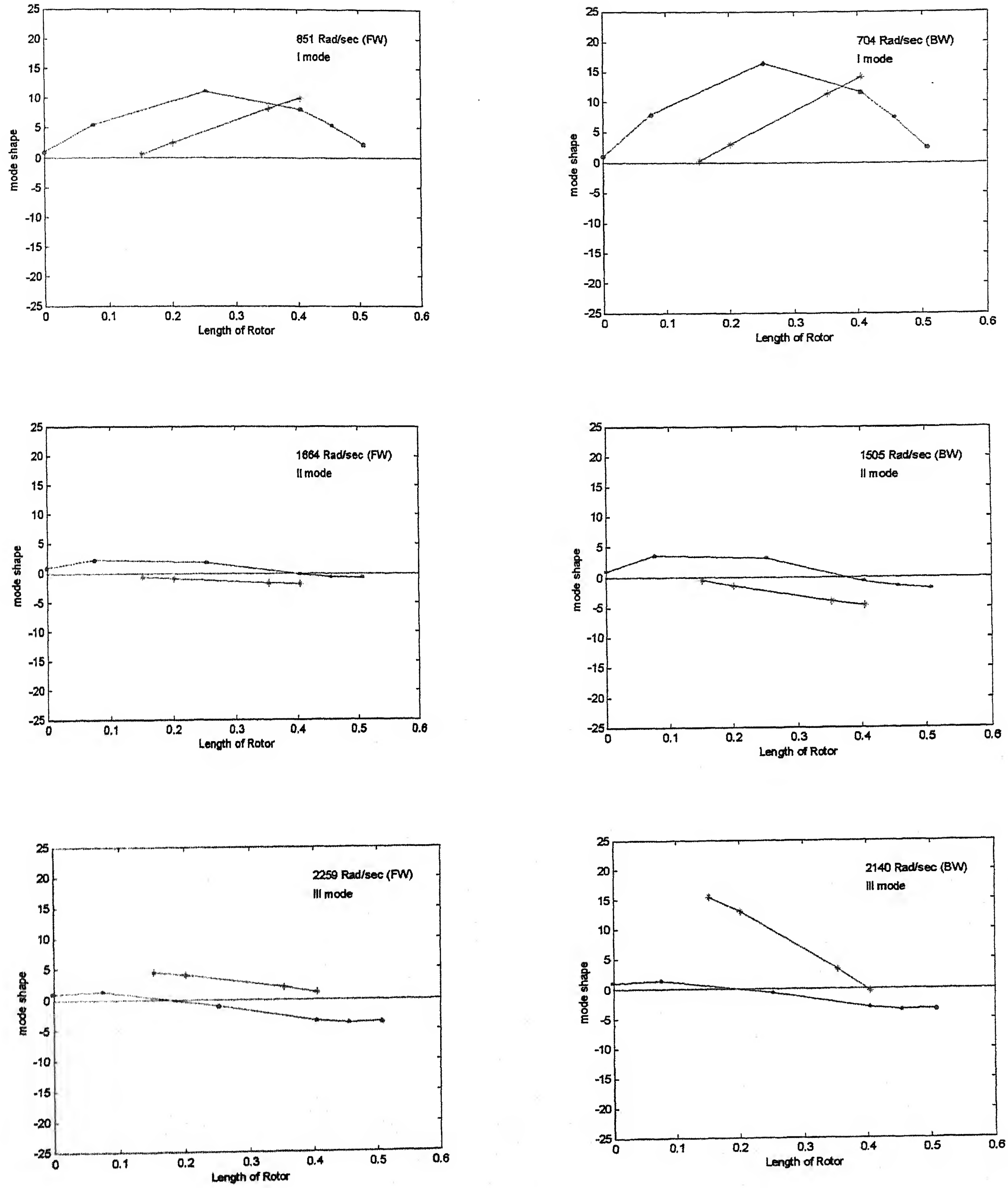

FW = Forward Whirl

BW = Backward Whirl

Figure 2.14(b) **Mode shapes corresponding to critical speeds (Case Study 2) (Synchronous whirl with outer rotor)**

Table2.5 (b) Critical Speeds (rad/s) - Synchronous whirl with outer rotor (Case Study 2)

Forward Whirl		Backward Whirl	
Rajan et al	Present Study (T.M.M.)	Rajan et al	Present Study (T.M.M.)
882	851	687	704
1584	1664	1462	1505
2274	2259	2175	2140

There is close resemblance between the results from the component synthesis method of Rajan et al and those from the transfer matrix method of the present study. The error can be reduced by increasing the number of stations in the transfer matrix model. The mode shapes corresponding to the critical speeds are shown in Figs. 2.14 (a), (b). It can be seen from these shape acquired by the rotor during forward and backward whirl is similar in a particular mode. However, the relative separation between the two rotors are different and is higher in backward whirl for the case investigated. The trend is similar for synchronous whirl with outer rotor and inner rotor. Further studies are required to describe the phenomenon in more detail.

Critical speeds have also been obtained for non-synchronous whirl of the rotor. These results are shown in Fig. 2.15 for the speed ratio of 1.5. The synchronous whirl critical speeds can be obtained from the intersection of straight lines *AB* and *AC* with the curves, for inner and outer rotors respectively.

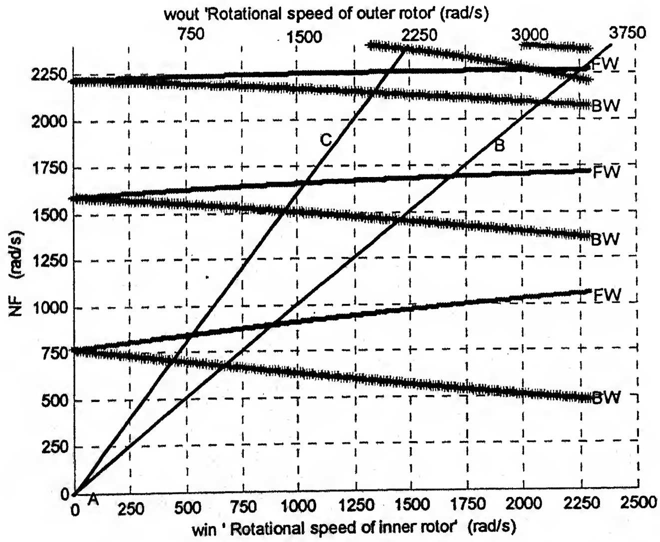

Figure 2.15 Natural frequencies (NF) and critical speeds of dual rotor

CHAPTER 3

UNBALANCE RESPONSE OF DUAL ROTOR

Residual unbalance is one of the most significant causes of excessive vibrations in rotating shafts. Unbalance primarily arises due to material inhomogeneities, manufacturing defects, keyways, slots etc. In addition deterioration due to wear and tear, thermal bending, process dirt collection etc. during operation also give rise to eccentricity between geometric and gravity centres, causing unbalanced forces. These can be removed by proper balancing procedure. It is important to determine response of the rotor due to unbalance, in order to study its dynamic behavior and set limits for safe operation.

3.1 Transfer Matrix Procedure

The extension of the transfer matrix procedure, discussed in the previous chapter, for unbalance response analysis of multi-spool rotors is described here (Rao, 1996).

3.1.1 Field Matrix

With reference to Fig 2.1-2.3 and accounting for bending in both *x-z* and *x-y* planes, the state vector {S} can be expressed as

$$\{S\} = \begin{Bmatrix} \{S_z\} \\ \{S_y\} \end{Bmatrix} \tag{3.1}$$

where

$$\{S_y\} = \begin{Bmatrix} v \\ \phi \\ M_z \\ -V_y \end{Bmatrix} \qquad \{S_z\} = \begin{Bmatrix} -w \\ \theta \\ M_y \\ V_z \end{Bmatrix} \tag{3.2}$$

It can be readily shown that

$$\{S_y\}_i^L = [F]_i \{S_y\}_{i-1}^R \tag{3.3}$$

where [F] is the same as defined previously by equation (2.8). Relations (2.8) and (3.3) can then be combined to give the overall state vector relation as follows

$$\begin{Bmatrix} \{S_z\} \\ \{S_y\} \end{Bmatrix}_i^L = \begin{bmatrix} [F] & [0] \\ [0] & [F] \end{bmatrix} \begin{Bmatrix} \{S_z\} \\ \{S_y\} \end{Bmatrix}_{i-1}^R \tag{3.4}$$

The unbalance mass in y-z plane is shown in Fig 3.1. The eccentricity, e_i at station i makes an angle β_i in $\bar{y}\bar{z}$ coordinates fixed to the rotor. The unbalance then is

$$u_{y,i} = m_i e_i \cos\beta_i; \qquad u_{z,i} = m_i e_i \sin\beta_i \tag{3.5}$$

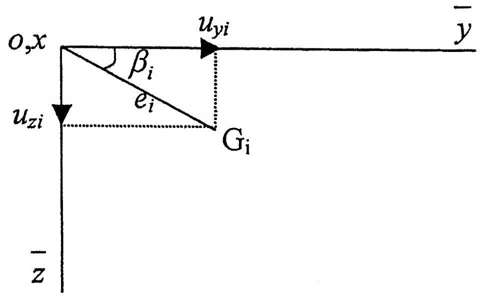

Figure 3.1 The *i*th unbalance mass

In general the response in the y-direction will be different from that in the z-direction. Further for anisotropic bearings the response in both the x-y and x-z planes will consist of sine and cosine components. Therefore splitting $\{S_z\}$ and $\{S_y\}$ further as

$$\{S_z\} = \begin{Bmatrix} \{S_{zc}\} \\ \{S_{zs}\} \end{Bmatrix}; \qquad \{S_y\} = \begin{Bmatrix} \{S_{yc}\} \\ \{S_{ys}\} \end{Bmatrix}$$

$$\{S_{zc}\} = \begin{Bmatrix} -w_c \\ \theta_c \\ M_{yc} \\ V_{zc} \end{Bmatrix}, \{S_{zs}\} = \begin{Bmatrix} -w_s \\ \theta_s \\ M_{ys} \\ V_{zs} \end{Bmatrix}, \{S_{yc}\} = \begin{Bmatrix} v_c \\ \phi_c \\ M_{zc} \\ -V_{yc} \end{Bmatrix}, \{S_{ys}\} = \begin{Bmatrix} v_s \\ \phi_s \\ M_{zs} \\ -V_{ys} \end{Bmatrix} \tag{3.8}$$

and adding the identity $1 \equiv 1$, to the 16 equations of total state vector for the purpose of response calculations, the overall field equation becomes

$$\begin{Bmatrix} \{S_{zc}\} \\ \{S_{zs}\} \\ \{S_{yc}\} \\ \{S_{ys}\} \end{Bmatrix}_I^L = \begin{bmatrix} [F] & [0] & [0] & [0] & \{0\} \\ [0] & [F] & [0] & [0] & \{0\} \\ [0] & [0] & [F] & [0] & \{0\} \\ [0] & [0] & [0] & [F] & \{0\} \\ \{0\}^T & \{0\}^T & \{0\}^T & \{0\}^T & 1 \end{bmatrix}_i \begin{Bmatrix} \{S_{zc}\} \\ \{S_{zs}\} \\ \{S_{yc}\} \\ \{S_{ys}\} \end{Bmatrix}_{i-1}^R \tag{3.9}$$

which is

$$\{\overline{S}\}_i^L = [\overline{F}]_i \{\overline{S}\}_{i-1}^R \tag{3.10}$$

where $\{\overline{S}\}$ and $[\overline{F}]$ are modified state vector and field matrix respectively.

3.1.2 Point Matrix

The free body diagram for the ith unbalance mass in the x-z plane is given in Fig 2.3. Noting that and similar expression can be written for x-y plane.

$$\begin{aligned} V_{z,i}^R &= V_{z,i}^L - m_i\omega^2 w_i - \omega^2 u_{z,i}\cos\omega t + \omega^2 u_{y,i}\sin\omega t \\ V_{y,i}^R &= V_{y,i}^L - m_i\omega^2 w_i - \omega^2 u_{y,i}\cos\omega t + \omega^2 u_{z,i}\sin\omega t \end{aligned} \tag{3.11}$$

the relationships across the ith mass are written as

$$\begin{Bmatrix} \{S_{zc}\} \\ \{S_{zs}\} \\ \{S_{yc}\} \\ \{S_{zc}\} \\ 1 \end{Bmatrix}_i^R = \begin{bmatrix} [P] & [0] & [0] & [0] & \{m_{zc}\} \\ [0] & [P] & [0] & [0] & \{m_{zs}\} \\ [0] & [0] & [P] & [0] & \{m_{yc}\} \\ [0] & [0] & [\dot{0}] & [P] & \{m_{ys}\} \\ \{0\}^T & \{0\}^T & \{0\}^T & \{0\}^T & 1 \end{bmatrix} \begin{Bmatrix} \{\dot{S}_{zc}\} \\ \{S_{zs}\} \\ \{S_{yc}\} \\ \{S_{ys}\} \\ 1 \end{Bmatrix}_i^L \tag{3.14}$$

where $[P]$ is the point matrix defined earlier in equation (2.10) with critical speed p replaced by rotational speed ω, and

$$\{m_{zc}\} = \begin{Bmatrix} 0 \\ 0 \\ 0 \\ -\omega^2 u_z \end{Bmatrix} \qquad \{m_{zs}\} = \begin{Bmatrix} 0 \\ 0 \\ 0 \\ \omega^2 u_y \end{Bmatrix} \qquad \{m_{yc}\} = \begin{Bmatrix} 0 \\ 0 \\ 0 \\ \omega^2 u_y \end{Bmatrix} \qquad \{m_{ys}\} = \begin{Bmatrix} 0 \\ 0 \\ 0 \\ \omega^2 u_z \end{Bmatrix}$$

Equation (3.14) can be written as

$$\{\overline{S}\}_i^R = [\overline{P}]_i \{\overline{S}\}_i^L \tag{3.15}$$

3.1.3 Bearing Matrix

The stiffness and damping properties of bearings are incorporated in the bearing matrix. Refering to the equilibrium relations across a bearing (Fig 3.3) the bearing transfer matrix is

$$\{\overline{S}\}_i^R = [B]_i \{\overline{S}\}_i^L \tag{3.16}$$

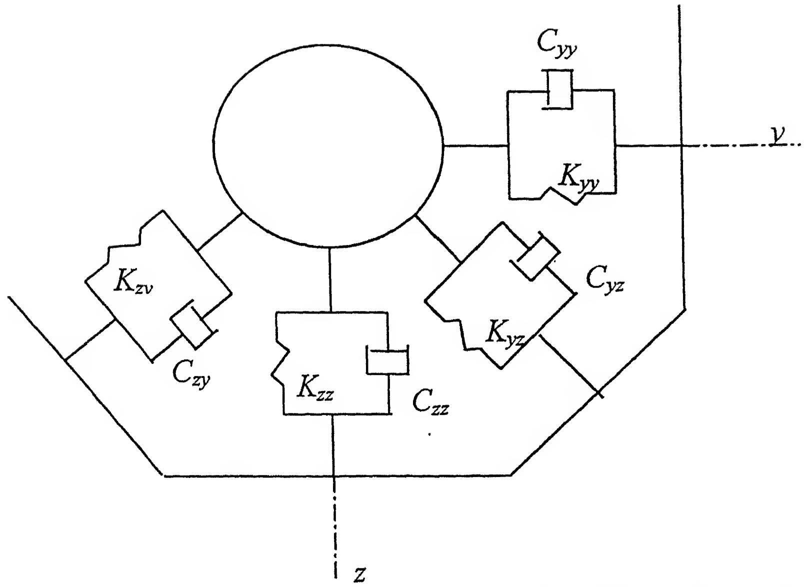

Figure 3.2 (a) **Stiffness and damping coefficients of the fluid film in bearing**

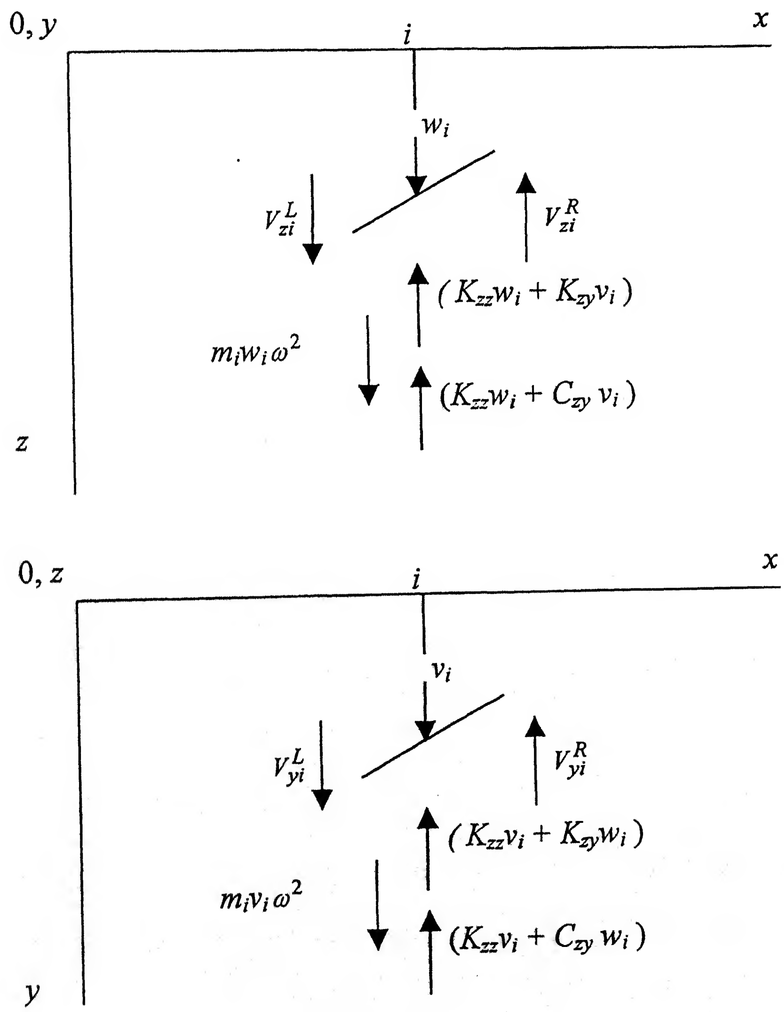

Figure 3.2 (b) **Equilibrium relations at bearing station**

where the non-zero elements of $[B]$ are

$$B_{r,s} = 1, r = s = 1,2.......,17 \qquad B_{12,9} = B_{16,13} = -K_{yy} + m\omega^2 \qquad B_{4,9} = B_{8,13} = -K_{zy}$$

$$B_{4,1} = B_{8,5} = -K_{zz} + m\omega^2 \qquad B_{4,5} = -B_{8,1} = -C_{zz}\omega \qquad B_{4,13} = -B_{8,9} = C_{zy}\omega$$

$$B_{4,13} = -B_{8,9} = C_{zy}\omega \qquad B_{12,5} = -B_{16,1} = C_{yz}$$

$$B_{12,1} = -B_{16,5} = K_{yz} \qquad B_{12,13} = -B_{16,9} = -C_{yy}\omega \tag{3.16a}$$

The overall transfer matrix of the rotor system mounted on fluid film bearings at both ends

$$\{\overline{S}\}^R_{n+1} = [B]_{n+1}[\overline{U}][B]_0\{\overline{S}\}^L_0 \tag{3.17}$$

$$\{\overline{S}\}^R_{n+1} = [\overline{U}_m]\{\overline{S}\}^L_0 \tag{3.18}$$

Where $[\overline{U}_m]$ is the overall transfer matrix of size 17x17, which includes bearings matrix also. For rotor with bearings at its both ends (the shear forces and bending moments are zero at both ends), one obtain the following

equation:

$$\begin{bmatrix} u_{3,1} & u_{3,2} & u_{3,5} & u_{3,6} & u_{3,9} & u_{3,10} & u_{3,13} & u_{3,14} \\ u_{4,1} & u_{4,2} & \cdots & & & & & u_{4,14} \\ u_{7,1} & & & & & & & \\ u_{8,1} & & & & & & & \\ u_{11,1} & & & & & & & \\ u_{12,1} & & & & & & & \\ u_{15,1} & & & & & & & \\ u_{16,1} & & \cdots & & & & & u_{16,14} \end{bmatrix} \begin{Bmatrix} -w_c \\ \theta_c \\ -w_s \\ \theta_s \\ v_c \\ \phi_c \\ v_s \\ \phi_s \end{Bmatrix}_0 = -\begin{Bmatrix} u_{3,17} \\ u_{4,17} \\ u_{7,17} \\ u_{8,17} \\ u_{11,17} \\ u_{12,17} \\ u_{15,17} \\ u_{16,17} \end{Bmatrix}$$

The above system of linear equation can be solved to determine $w_c, \theta_c etc.$, at the zeroth station, which will define $\{\overline{S}\}^L_0$. The state vectors at all other stations are then obtained using appropriate transfer matrices to get the unbalance response of rotor.

3.1.4 Modifications for Dual Rotor

In a dual rotor presence of intershaft bearings requires modification in the state vector with field and point matrix, since the dynamic response of each rotor not only depends upon its own unbalance but also the dynamic behavior of other. Therefore, each quantity of the state vector requires to have two components, one corresponding to inner rotor speed and other to outer rotor speed. If the suffixes m and n represents the inner and outer rotors respectively, ω_m - inner rotor speed, ω_n - outer rotor speed etc. Then for x-z plane we have

$$\begin{aligned}
w &= w_{cm}\cos\omega_m t + w_{sm}\sin\omega_m t + w_{cn}\cos\omega_n t + w_{sn}\sin\omega_n t \\
\theta &= \theta_{cm}\cos\omega_m t + \theta_{sm}\sin\omega_m t + \theta_{cn}\cos\omega_n t + \theta_{sn}\sin\omega_n t \\
M_y &= M_{ycm}\cos\omega_m t + M_{ysm}\sin\omega_m t + M_{ycn}\cos\omega_n t + M_{ysn}\sin\omega_n t \\
V_z &= V_{zcm}\cos\omega_m t + V_{zsm}\sin\omega_m t + V_{zcn}\cos\omega_n t + V_{zsn}\cos\omega_n t
\end{aligned} \tag{3.19}$$

Similar expressions can be written for the x-y plane and the state vector is modified to contain 33 quantities

$$\{S\} = \{\{S_{zm}\} \quad \{S_{zn}\} \quad \{S_{ym}\} \quad \{S_{yn}\} \quad 1\}^{T} \tag{3.20}$$

where

$$\{S_{zm}\} = \begin{Bmatrix} -w_{cm} \\ \theta_{cm} \\ M_{ycm} \\ V_{zcm} \\ -w_{sm} \\ \theta_{sm} \\ M_{ysm} \\ V_{zsm} \end{Bmatrix}, \{S_{zn}\} = \begin{Bmatrix} -w_{cn} \\ \theta_{cn} \\ M_{ycn} \\ V_{zcn} \\ -w_{sn} \\ \theta_{sn} \\ M_{ysn} \\ V_{zsn} \end{Bmatrix}, \{S_{ym}\} = \begin{Bmatrix} v_{cm} \\ \phi_{cm} \\ M_{zcm} \\ V_{ycm} \\ v_{sm} \\ \phi_{sm} \\ M_{zsm} \\ V_{ysm} \end{Bmatrix}, \{S_{yn}\} = \begin{Bmatrix} v_{cn} \\ \phi_{cn} \\ M_{zcn} \\ V_{ycn} \\ v_{sn} \\ \phi_{sn} \\ M_{zsn} \\ V_{ysn} \end{Bmatrix} \tag{3.21}$$

Now it can be readily shown that corresponding field matrix is given by

$$[F]_{33x33}=\begin{bmatrix} [F] & 0 & 0 & 0 & 0 & 0 & 0 & 0 & 0 \\ 0 & [F] & 0 & 0 & 0 & 0 & 0 & 0 & 0 \\ 0 & 0 & [F] & 0 & 0 & 0 & 0 & 0 & 0 \\ 0 & 0 & 0 & [F] & 0 & 0 & 0 & 0 & 0 \\ 0 & 0 & 0 & 0 & [F] & 0 & 0 & 0 & 0 \\ 0 & 0 & 0 & 0 & 0 & [F] & 0 & 0 & 0 \\ 0 & 0 & 0 & 0 & 0 & 0 & [F] & 0 & 0 \\ 0 & 0 & 0 & 0 & 0 & 0 & 0 & [F] & 0 \\ 0 & 0 & 0 & 0 & 0 & 0 & 0 & 0 & 1 \end{bmatrix} \tag{3.22}$$

where $[F]$ is the field matrix derived in section 2.1. Also the point matrix can be seen to be readily modified to

$$[P]_{33x33}=\begin{bmatrix} [P_m] & 0 & 0 & 0 & \{m_{zm}\} \\ 0 & [P_n] & 0 & 0 & \{m_{zn}\} \\ 0 & 0 & [P_m] & 0 & \{m_{ym}\} \\ 0 & 0 & 0 & [P_n] & \{m_{yn}\} \\ 0 & 0 & 0 & 0 & 1 \end{bmatrix} \tag{3.23}$$

where

$$[P_m]=\begin{bmatrix} [P] & 0 \\ 0 & [P] \end{bmatrix}_{p=\omega_m}, [P_n]=\begin{bmatrix} [P] & 0 \\ 0 & [P] \end{bmatrix}_{p=\omega_n}$$

For inner rotor $\{m_{zn}\}$ and $\{m_{yn}\}$ will be null matrix and $\{m_{zm}\}, \{m_{ym}\}$ will be given by equation (3.24).

$$\{m_{zm}\}=\{0\ 0\ 0\ \ -u_z\omega_m^2\ 0\ 0\ 0\ \ u_y\omega_m^2\}^T$$

$$\{m_{ym}\}=\{0\ 0\ 0\ \ u_y\omega_m^2\ 0\ 0\ 0\ \ u_z\omega_m^2\}^T \tag{3.24}$$

and $[P]$ is given by equation (2.10). If the gyroscopic couple is to be taken in account, $[P]$ in the above equation can be taken from the equation (2.24). Similar

expressions can be written for the outer rotor. Also, the bearing matrix gets modified to

$$[\boldsymbol{Be}]=\begin{bmatrix} [Be_{mz1}] & 0 & [Be_{mz2}] & 0 & 0 \\ 0 & [Be_{nz1}] & 0 & [Be_{nz2}] & 0 \\ [Be_{my2}] & & [Be_{my1}] & 0 & 0 \\ 0 & [Be_{ny2}] & 0 & [Be_{ny1}] & 0 \\ 0 & 0 & 0 & 0 & 1 \end{bmatrix} \tag{3.25}$$

where non zero terms of sub matrices are

$$[Be_{mz1}](i,i)=1, i=1,2,.....8$$
$$[Be_{mz1}](4,1)=[Be_{mz1}](8,5)=-K_{zz}+m\omega_m^2$$
$$[Be_{mz1}](4,5)=-C_{zz}\omega_m$$
$$[Be_{mz1}](8,1)=C_{zz}\omega_m$$

$$[Be_{mz2}](4,1)=[Be_{mz2}](8,5)=-K_{zy}$$
$$[Be_{mz2}](4,5)=C_{zy}\omega_m$$
$$[Be_{mz2}](8,1)=-C_{zy}\omega_m$$

Matrices $[Be_{my1}]$ and $[Be_{my2}]$ are obtained from the above by replacing subscripts z with y and y with z. Similarly one can get the other sub matrices used in bearing matrix.

3.1.5 Junction conditions

With reference to Fig. 3.3 if [A], [B], [C] and [D] represent the overall transfer matrix considering all the stations between the starting station zero, for the A, B, C and D shaft sections and the junction point where the intershaft bearing is located, then

$$\{S\}_{mj}^{L}=[A]\{S\}_{0A} \qquad \{S\}_{0B}=[B]\{S\}_{mj}^{R}$$
$$\{S\}_{nj}^{L}=[C]\{S\}_{0C} \qquad \{S\}_{0D}=[D]\{S\}_{nj}^{R} \qquad [Be]=[\boldsymbol{Be}]-[I] \tag{3.26}$$

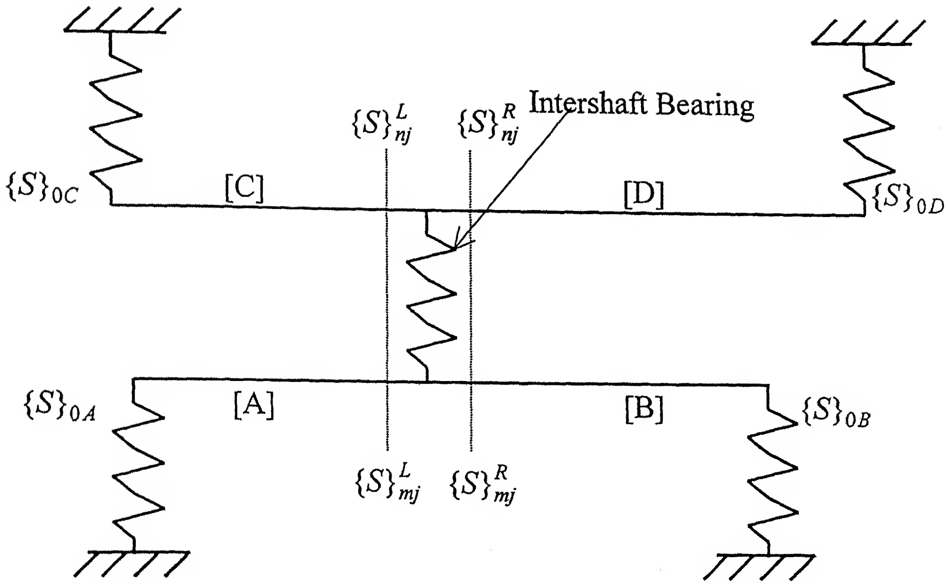

Figure 3.3 Junction Conditions

At the junction of the inner rotor, one gets

$$\{S\}_{mj}^{R} = [I]\{S\}_{mj}^{L} + [Be]\{S\}_{mj}^{L} - [Be]\{S\}_{nj}^{L} \tag{3.27}$$

Similarly at the junction of outer rotor

$$\{S\}_{nj}^{R} = [I]\{S\}_{nj}^{L} + [Be]\{S\}_{nj}^{L} - [Be]\{S\}_{mj}^{L} \tag{3.28}$$

Substituting $\{S\}_{mj}^{R}$ and $\{S\}_{nj}^{R}$ from the above in the second and fourth equation of (3.26),

$$\begin{aligned} \{S\}_{0B} &= [B][[I]+[Be]]\{S\}_{mj}^{L} - [B][Be]\{S\}_{nj}^{L} \\ \{S\}_{0D} &= [D][[I]+[Be]]\{S\}_{nj}^{L} - [D][Be]\{S\}_{mj}^{L} \end{aligned} \tag{3.29}$$

With the help of first and third equations of (3.26), the above can be written as

$$\begin{aligned} \{S\}_{0B} &= [B][[I]+[Be]][A]\{S\}_{0A} - [B][Be][C]\{S\}_{0C} \\ \{S\}_{0D} &= [D][[I]+[Be]][C]\{S\}_{0C} - [D][Be][A]\{S\}_{0A} \end{aligned} \tag{3.30}$$

Premultiplying the first equation by $[B]^{-1}$ and second equation by $[D]^{-1}$, the above equation can be written in one matrix equation.

$$\begin{bmatrix} [A_m] & [B_m] & [C_m] & [0] \\ [A_n] & [0] & [C_n] & [D_n] \end{bmatrix}_{66x132} \begin{Bmatrix} \{S\}_{0A} \\ \{S\}_{0B} \\ \{S\}_{0C} \\ \{S\}_{0D} \end{Bmatrix}_{132x1} = 0 \qquad (3.31)$$

where

$$[A_m] = [[I] + [Be]][A]$$
$$[B_m] = -[B]^{-1}$$
$$[C_m] = -[Be][C]$$
$$[A_n] = -[Be][A]$$
$$[C_n] = [[I] + [Be]][C]$$
$$[D_n] = -[D]^{-1}$$

If the intershaft bearing matrix is unit matrix, it can be seen that equation (3.31) reduces to two uncoupled equation for the outer and inner rotors. For free end boundary conditions at the four ends of dual rotor system, all moments and shear forces are assumed to be zero, i.e., at these ends,

$$M_{ym} = M_{yn} = M_{zm} = M_{zn} = 0$$
$$V_{ym} = V_{yn} = V_{zm} = V_{zn} = 0$$

The unknown quantities are w, θ, v, ϕ at the four starting stations. For each starting station there are 16 unknowns

$$\{\underline{S}\}_{0A} = \{-w_{cm}, \theta_{cm}, -w_{sm}, \theta_{sm}, ..., v_{sn}, \phi_{sn}\}_{0A}^{T}$$

and similarly $\{\underline{S}\}_{0B}, \{\underline{S}\}_{0C}$ and $\{\underline{S}\}_{0D}$ be the unknown quantities at the starting stations of all four section. Since M_y, V_z etc. terms in the vector of equation are zero. Columns 3,4,7,8,11,12, ...31,32; 36,37...64,65; 69,70...97,98; 102,103.....130,131; can be dropped in the 66x132 matrix of equation. The 33rd, 66th , 99th and 132nd elements of vector are unity and hence when multiplied with the corresponding column quantity in the matrix, give rise to a constant quantity independent of any

state vector dynamic quantity. These four terms can be added and taken to the right hand side of the corresponding equation. 33rd and 66th rows of the equation (3.31) can be deleted as they simply give identity equations. Then the equations (3.31) reduce to

$$[\overline{A}]_{64x64}\{S_O\}_{64x1} = \{\overline{B}\}_{64x1} \tag{3.32}$$

where

$$\{S_O\} = \begin{Bmatrix} \{\underline{S}\}_{OA} \\ \{\underline{S}\}_{OB} \\ \{\underline{S}\}_{OC} \\ \{\underline{S}\}_{OD} \end{Bmatrix} \tag{3.33}$$

$$\overline{B}_i = A_{mi,33} + B_{mi,33} + C_{mi,33} + D_{mi,33}$$

and $\overline{A}(i,j)$ are the elements picked up from the matrix (3.31) as described in the above manner, by dropping columns 3,4,7,8 etc., and rows 33 and 66.

The linear system of equation (3.32) can be solved to obtain $\{S_0\}$ in (3.33). From there, the state vector quantities at any station can e determined using the appropriate transfer matrices.

The response of a straight rotor is characterized by superposition of two perpendicular harmonic motions with the same angular frequency, which gives rise to an elliptical motion. However, for dual rotors, the unbalance response comprises of two different frequency components, belonging to the inner and outer rotors running speeds. In such a case, the sum of the different harmonic functions will be a periodic function if the ratio of the two frequencies is a rational number, and beating phenomenon will be observed with the an angular frequency given by the largest common divisor of both frequencies. (Rossing et.al. 1995), The period of such a beating phenomenon is

$$T = 2\pi(p-q)/(\omega_n - \omega_m), \tag{3.34}$$

where p and q are the smallest integers such that $p/q = \omega_n/\omega_m$. The superposition of the response components w and v leads to a motion characterized by a closed

periodic orbit, with a number of loops. The number of such loops is given $n = \{Max[\omega_n, \omega_m]\}(p - q)/(\omega_n - \omega_m)$. (3.35)

The algorithm for unbalance response computation has been developed in MATLAB and verified with the results of a case study taken up by Gupta et al (1988).

3.2 Case Study 3

The extended transfer matrix method for dual rotor described above, is illustrated through the idealized dual rotor model mounted on isotropic bearings as shown in Fig.-3.4. The shaft diameter is 1.5 cm and the Young's modulus is taken as 210×10^9 N/m^2. The unbalance on each mass is in phase with the other and is equal to 0.001-kg m. The speed of inner rotor is 1200 rpm and outer rotor is 1000 rpm. As discussed earlier, the response of each rotor, will be affected by the unbalance of its own as well as the other rotor. The total response at any speed to be the sum of two harmonic components, in present case with 1200 rpm and 1000 rpm frequencies, giving rise to a beating phenomenon. The whirl orbit for disc 1and 2 of both rotor at specified speed ratio is shown in Fig.3.5.

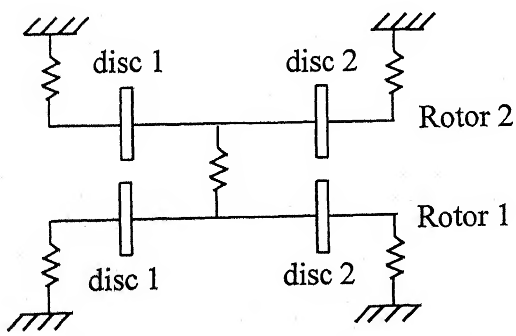

Figure 3.4 Idealized dual rotor model

The first two natural frequencies of the present dual rotor model can be computed to be 238 rad/s (2273 rpm) and 539 rad/s (5147 rpm). The unbalance response has been computed for two sets of inner and outer rotor speeds. The first set is chosen as 2500 rpm for the inner rotor and 2000 rpm for the outer rotor. This set lies close to the first natural frequency. The other set of inner and outer rotor speeds is chosen as 5500 rpm and 5000 rpm, so that the operation is closer to the second natural frequency. For the

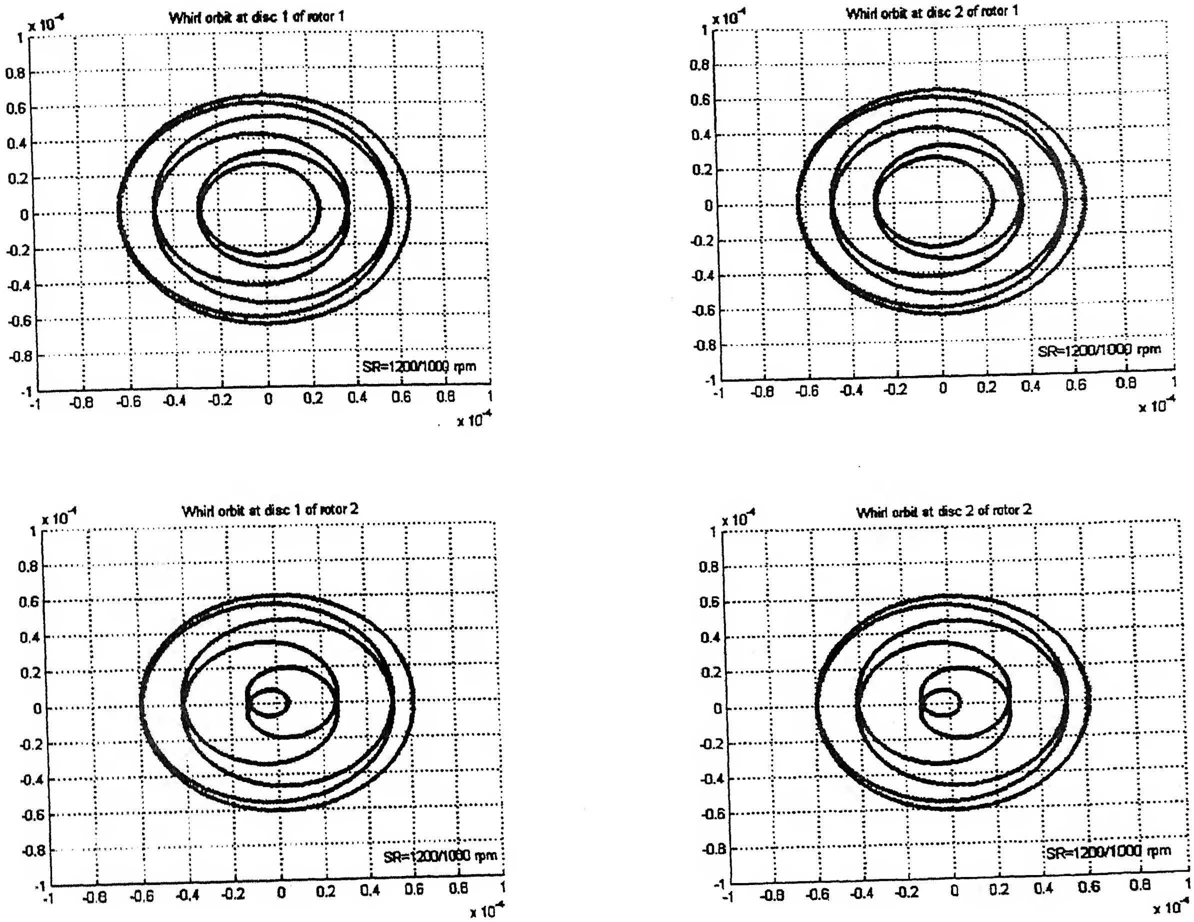

Figure 3.5 **Whirl orbits at speed ratio of 1200 rpm/1000 rpm**

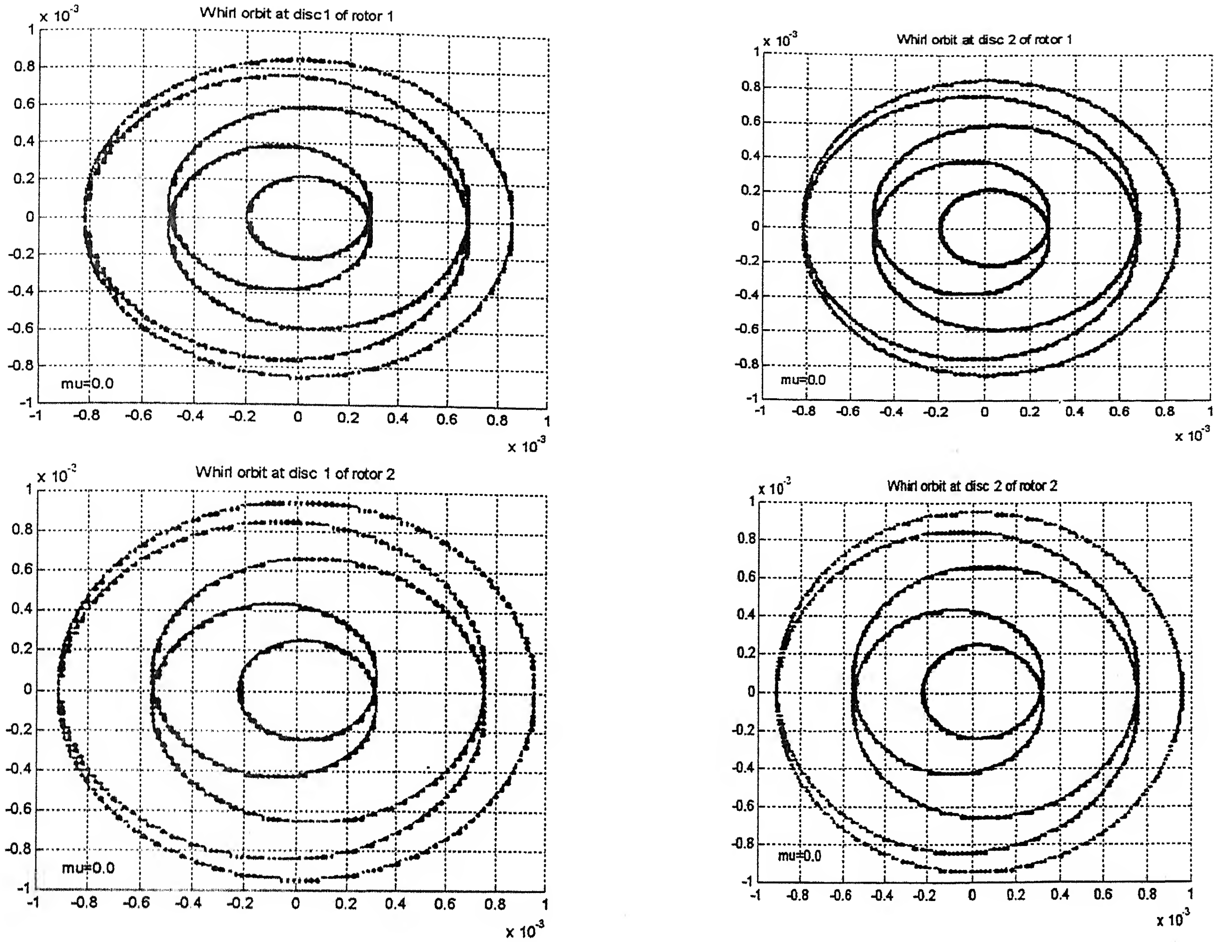

Figure 3.6 Whirl orbits at speed ratio of 2500rpm/2000 rpm

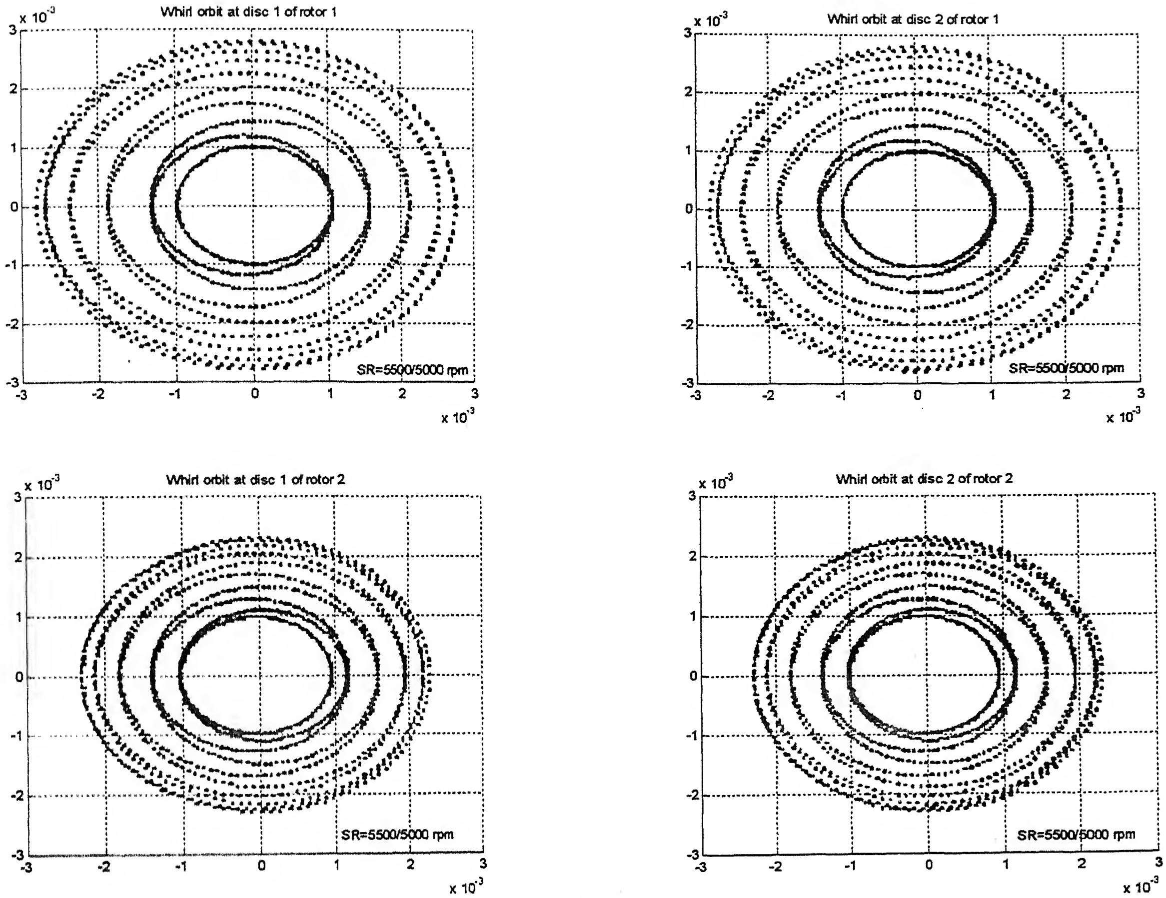

Figure 3.7 Whirl orbits at speed ratio of 5500 rpm/5000 rpm for Dual rotor

first set of speeds $p/q = 5/4$, $T = 0.12$ s and $n = 5$. For the second set, we have $p/q = 11/10$, $T = 0.12$ s and $n = 11$.The unbalance response in the two cases is shown in Figs. 3.6 and Figs 3.7, respectively. It can be seen that the orbits traced out by the inner and outer rotors at the two speeds are different in many ways. This dynamic behaviour would be dependent on a variety of design factors and operating speed regimes. An attempt has been made in the present study to investigate one such design parameter, i.e. the cross-coupling effects of the intershaft bearing. This is discussed in the next section.

3.3 Influence of Cross-Coupling Stiffness of the Intershaft bearing

The influence of the value of the cross-coupling stiffness of the intershaft bearing on the unbalance whirl orbit has been investigated by defining the cross coupling parameters

$\mu_1 = k_{yz} / k_{yy}$ and

$$\mu_2 = k_{zy} / k_{zz} \tag{3.36}$$

For the present study the two parameters have been taken to be equal, i.e. $\mu_1 = \mu_2 = \mu$. Retaining all parameters, from the previous section, including $k_{yy} = k_{zz} = 1.0$ MN/m, the values of cross-coupling terms k_{yz} k_{zy} are varied to obtain whirl orbits for $\mu = 0.0,\ 0.5,\ 1.0$. These orbits are shown in Figs. 3.8 and 3.9 for two speed ratios used earlier, namely 2500rpm / 2000rpm and 5500rpm/5000rpm. It can be seen from these figures that cross-coupling values play a more critical role in determining the unbalance locus of the rotor, for the second set of speeds. The first set of speeds is in the vicinity of the first mode of the rotor, whereby both shafts are moving in phase. The second set of speeds is in the vicinity of the second mode, whereby the two shafts move in opposite phase and more transfer of energy takes place through the intershaft spring. Role of the cross-coupling parameter μ is more critical here as evidenced in Fig.3.9. Also, for both sets of speeds increase in cross-coupling results, in increase of the skewness of the orbit. A reduction in the orbit amplitude is also visible, with increase in μ - a result of increased system stiffness.

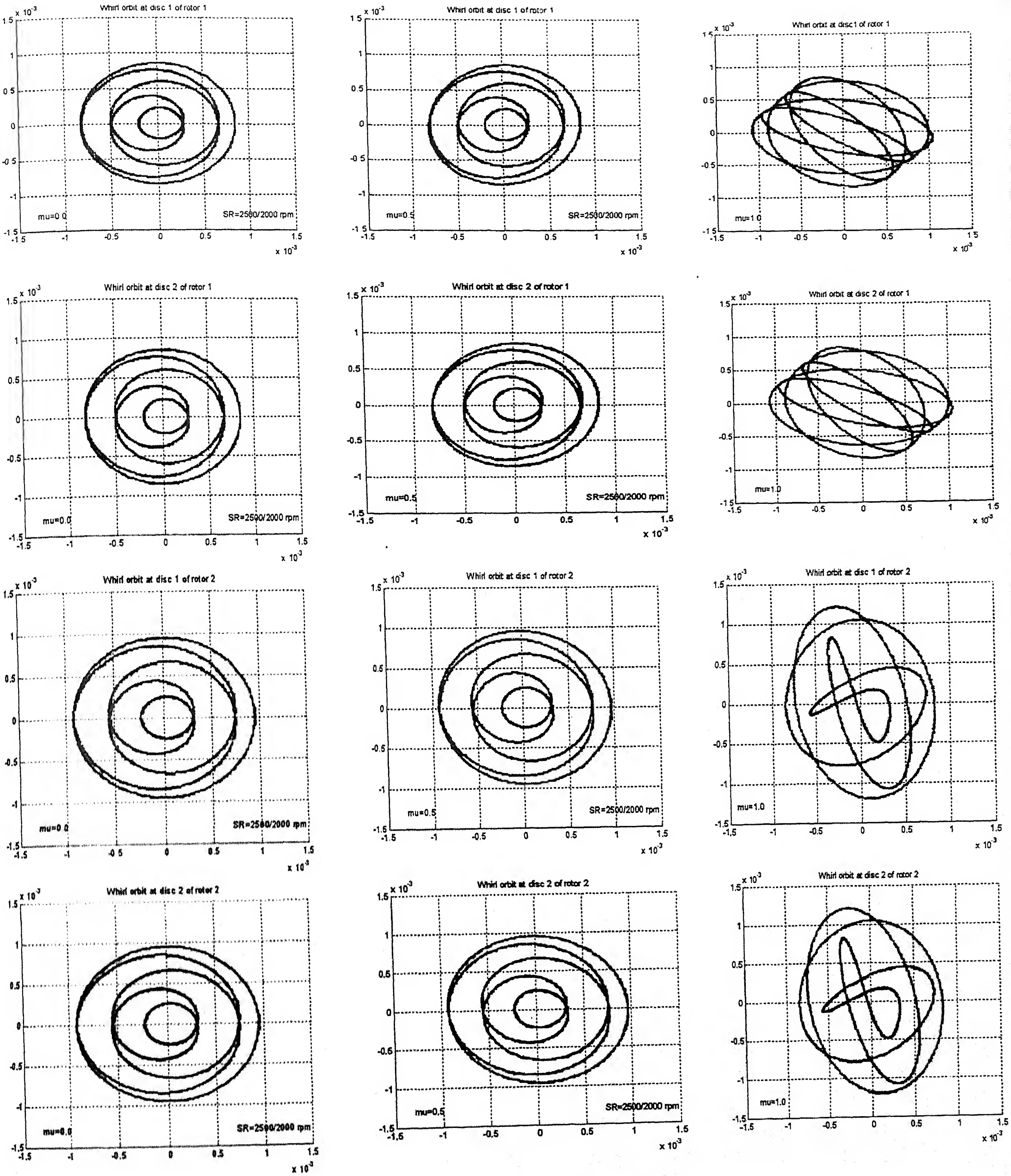

Figure 3.8 Whirl orbits at speed ratio of 2500rpm/2000 rpm ($\mu = 0.0, 0.5, 1.0$)

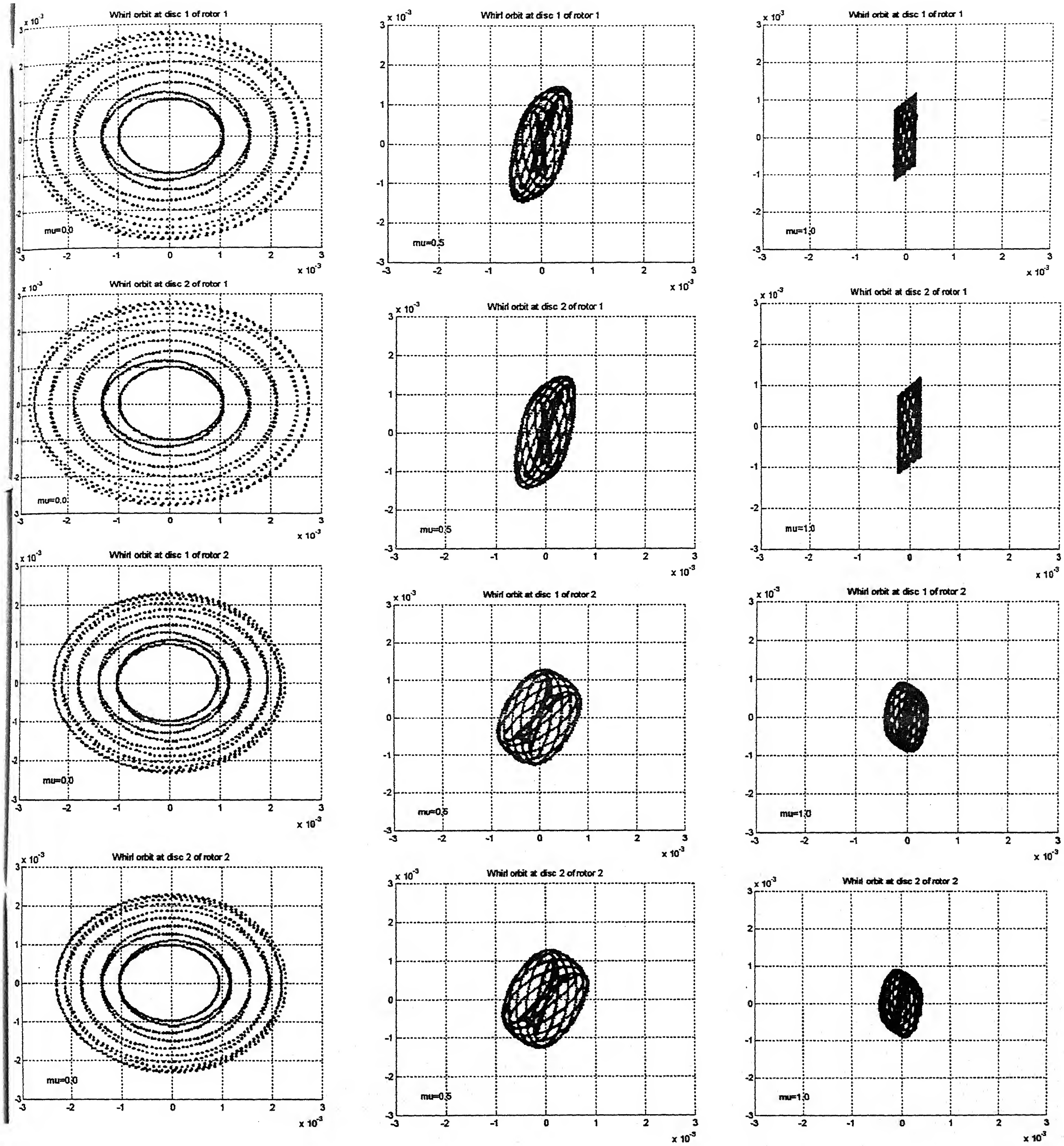

Figure 3.9 Whirl orbits at speed ratio of 5500 rpm/5000 rpm (μ=0.0,0.5,1.0)

No attempt has been made in the present study, to investigate the influence of intershaft damping. A comprehensive analysis of the dynamics of multi-spool rotors and its dependence on various shaft geometry parameters, speeds and speed ratios, bearing locations, stiffness and damping parameters requires more exhaustive simulation.

CHAPTER 4

DYNAMIC ANALYSIS OF AEROENGINE ROTOR

In this chapter, some aspects of the dynamics of an aeroengine rotor are attempted to be analysed. A typical aeroengine rotor with two shafts is chosen for study. The inner shaft carrying the LP stages of the the compressor and turbine at its two ends and supports the outer rotor in its central portion, through two intershaft bearings. Free vibration analysis is carried out using - both the transfer matrix procedure and FEM package. Residual unbalance response is computed using transfer matrix procedure.

4.1 Stage Data

The aeroengine rotor is schematically shown in Fig. 4.1. The outer rotor carries the HP stages of the compressor and turbine. The compressor comprises of 5 LP stages and 6 HP stages, while the turbine comprises of one LP and HP stage, each. The various stages are modeled as discs. Most of the data is mentioned on the Fig.4.1 itself. Some other relevant features are listed in Table 4.1.

Table 4.1 Aeroengine rotor Disc Diameters

Component Name	Stage No.	Outer Diameter (mm)
Inlet vane	–	800
L.P. Compressor	1	800
	2	720
	3	640
	4	560
	5	480
H.P. Compressor	1 – 6	400
H.P. Turbine	1	800
L.P. Turbine	1	575

Young's modules (E) 210×10^9 N/m^2 Density 8304 Kg/m^3

(material properties of all parts are taken as same in the present model)

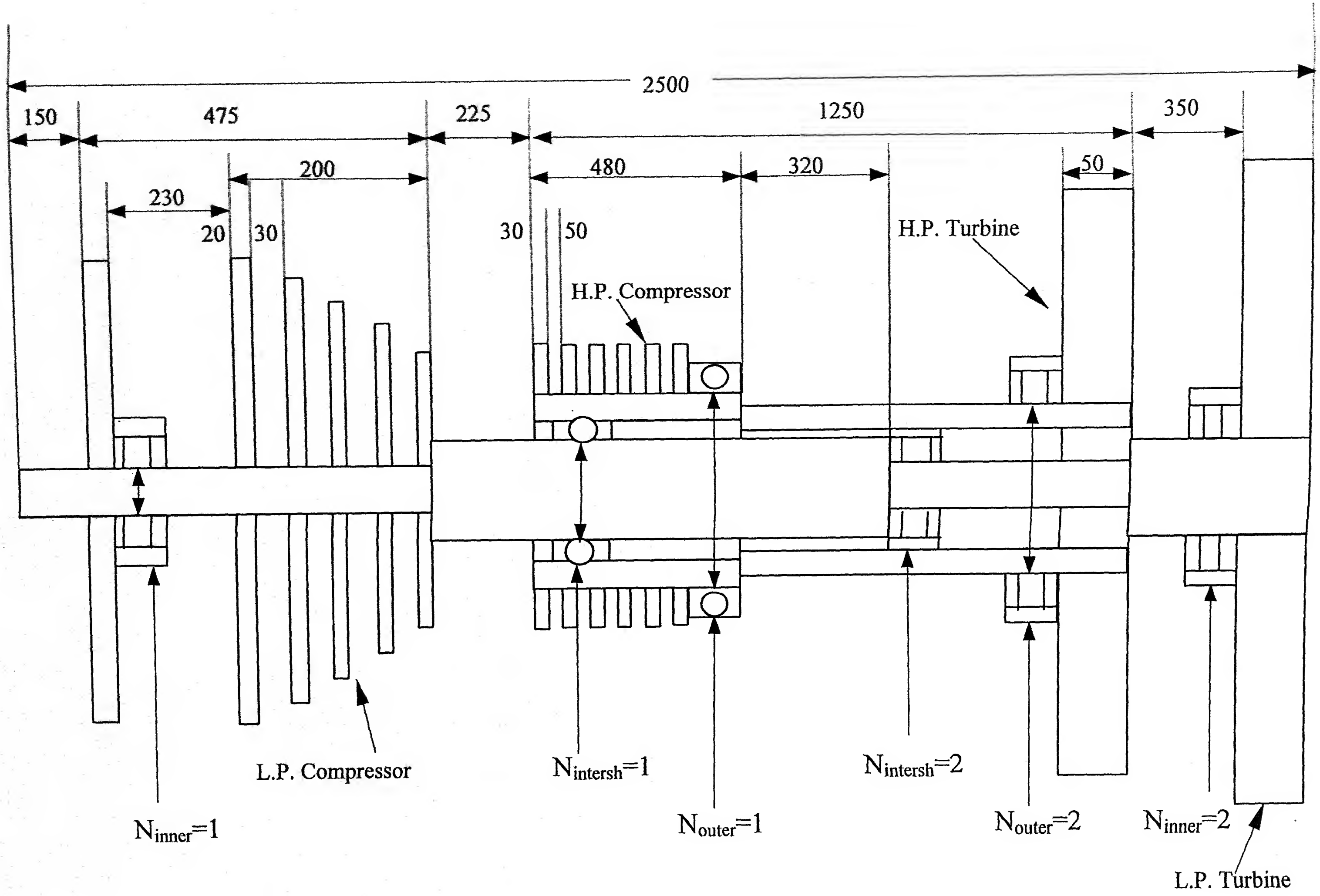

Figure 4.1 AEROENGINE

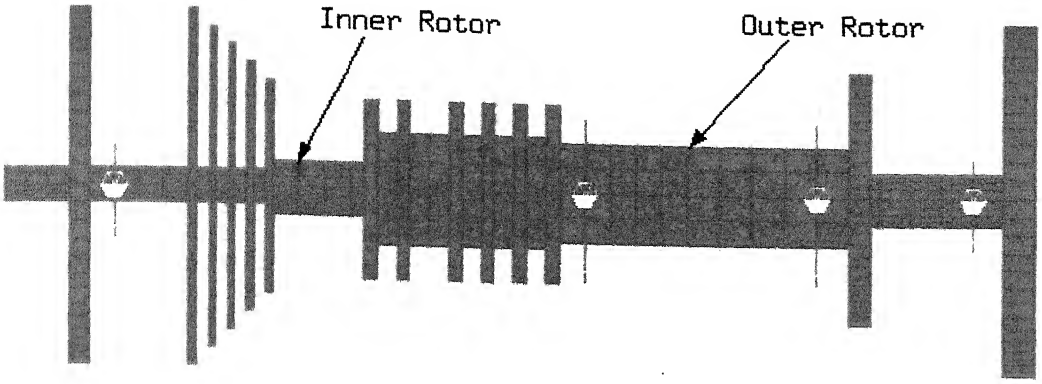

Figure 4.2 3D Finite Element Model of Aeroengine Rotor

4.2 Bearing Data and Stiffness Computation

The bearings supporting the inner and outer rotors and the intershaft bearing, in the aeroengine rotor are all rolling element types. Data for the typical bearings chosen for this case study are given here (refer Fig. 4.1).

The bearings have modeled as two translational springs, one in each y and z direction. Cross-coupling effects and damping are neglected, since these effects are small in case of ball bearings. Stiffness computation is done by employing the procedures outlined by Harris (1966), based on the extension of Hertzian contact theory. The procedure is briefly described here.

The total elastic force at the point of contact of the kth ball with the inner or outer races is expressed as

$$F_k = K_n(g + x\cos\eta_k + y\sin\eta_k)^{3/2} \tag{4.1}$$

and its projection along the line of action of applied force is

$$F_k = K_n(g + x\cos\eta_k + y\sin\eta_k)^{3/2}\cos\eta_k \tag{4.2}$$

where g is the radial preload or the radial pre-clearance between the ball and the races and x and y are the displacements of the moving ring in the direction of radial load and perpendicular to the direction of radial load respectively. η_k is the angle between the line of action of the radial load (direction of displacement of the moving ring) and the radius passing through the center of the kth ball. K_n is a coefficient of

Table 4.2 Bearing Specifications

Bearing No.	Type of bearing	No. of rollers/balls	Roller/Ball dia (mm)	Inner race dia (mm)	Outer race dia. (mm)	Roller Length (mm)	Radial Clear - - ance (mm)x10^{-3}
$N_{inner}1$	Roller	22	09.5	080.0	140.0	25.0	0.085 -0.115
$N_{inner}2$	Roller	30	11.0	120.0	215.0	40.0	0.095 –0.130
$N_{outer}1$	Ball	29	35.0	225.0	405.0	-	0.150 - 0.190
$N_{outer}2$	Roller	30	15.0	150.0	270.0	55.0	0.030 – 0.080
$N_{intersh}1$	Ball	21	24.0	120.0	215.0	-	0.110 - 0.160
$N_{intersh}2$	Roller	36	06.0	080.0	140.0	25.0	0.045 – 0.142

proportionality depending on the geometric and material properties of the bearing. The coefficient of proportionality is estimated by the method suggested by Harris (1966), as follows. Writing equation (4.1) as in general for ball bearing.

$$F = K_n \delta^{3/2} \text{ (the exponential value is 1.11 for roller bearings)} \qquad (4.3)$$

where δ is defined as a deflection.

and since he total normal approach between two raceways under load separated by a rolling element is the sum of the approaches between the rolling element and each raceway, i.e. $\delta_k = \delta_{k_i} + \delta_{k_o}$

Therefore

$$K_n = [1/((1/K_i)^{1/n} + (1/K_o)^{1/n})]^n \qquad (4.3)$$

and

$$F = K_n \delta^n \qquad (4.4)$$

For steel ball-steel raceway contact,

$$K_{i,o} = 2.15x10^5 \Sigma\sigma^{-1/2}(\delta^*)^{-3/2} \qquad (4.5a)$$

and for steel roller and raceway contact,

$$K_{i,o} = 0.786x10^5 l^{8/9} \qquad (4.5b)$$

where $\Sigma\sigma$ is curvature sum and δ^* is dimensionless deflection or contact deformation and is a function of the curvature difference $\partial\sigma$ and l is roller length. (Harris, 1966). Curvature sum for ball-inner ring raceway and for ball-outer ring raceway can be calculated from the following set of equations.

$$\Sigma\sigma_i = \frac{1}{D}\left(4 - \frac{1}{f_i} + \frac{2\gamma}{1-\gamma}\right) \qquad \Sigma\sigma_0 = \frac{1}{D}\left(4 - \frac{1}{f_0} - \frac{2\gamma}{1+\gamma}\right) \qquad f = \frac{1}{2\varphi} = \frac{r}{D}$$

$$\gamma = \frac{D\cos\alpha}{d_m} \qquad \partial\sigma_i = \frac{\frac{1}{f_i} + \frac{2\gamma}{1-\gamma}}{4 - \frac{1}{f_i} + \frac{2\gamma}{1-\gamma}} \qquad \partial\sigma_o = \frac{\frac{1}{f_0} - \frac{2\gamma}{1+\gamma}}{4 - \frac{1}{f_o} - \frac{2\gamma}{1+\gamma}} \qquad (4.6)$$

The total elastic force in the direction of the applied force is (refer equation 4.2)

$$F = \sum_{k=1}^{n} F_k \tag{4.9}$$

where n is the total number of balls in the bearings.

Using the condition of zero elastic force in the direction perpendicular to the elastic load, the deformation y, perpendicular to the radial force line is expressed as

$$y = \frac{\sum_{k=1}^{n} [g + x\cos\eta_k]^{3/2} \sin\eta_k}{\sum_{k=1}^{n} [g + x\cos\eta_k]^{1/2}} \sin^2\eta_k \tag{4.10}$$

The bearing stiffness is determined as the function of the deformation x as

$$k(x) = \frac{\partial F}{\partial x} \tag{4.11}$$

Stiffness values thus calculated, for various bearings on the aeroengine rotor are listed in Table 4.3. The bearing is assumed to be isotropic, with identical stiffness in all radial directions. Cross-coupling influences in rolling element bearings are generally negligible. Damping is also small in these bearings and is ignored in the present model.

Table 4.3 Bearing Stiffness

Bearing Number	Bearing Stiffness (N/mm)
N_{inner} 1	$2.6240\text{x}10^6$
N_{inner} 2	$5.7600\text{x}10^6$
N_{outer} 1	$0.1096\text{x}10^6$
N_{outer} 2	$7.0480\text{x}10^6$
$N_{intersh}$ 1	$0.0915\text{x}10^6$
$N_{intersh}$ 2	$2.6240\text{x}10^6$

4.3 Natural frequencies and Mode shapes

The FE model of aeroengine rotor, using 3D solid hexahedral elements is shown in Fig.4.2. Free vibration analysis is carried out using NISA software as well as the transfer matrix algorithm in MATLAB. A comparison between the two sets of results is given in Table 4.4. The natural frequencies from the two procedures are fairly close, the difference primarily arising from the discretisation process in Transfer matrix method.

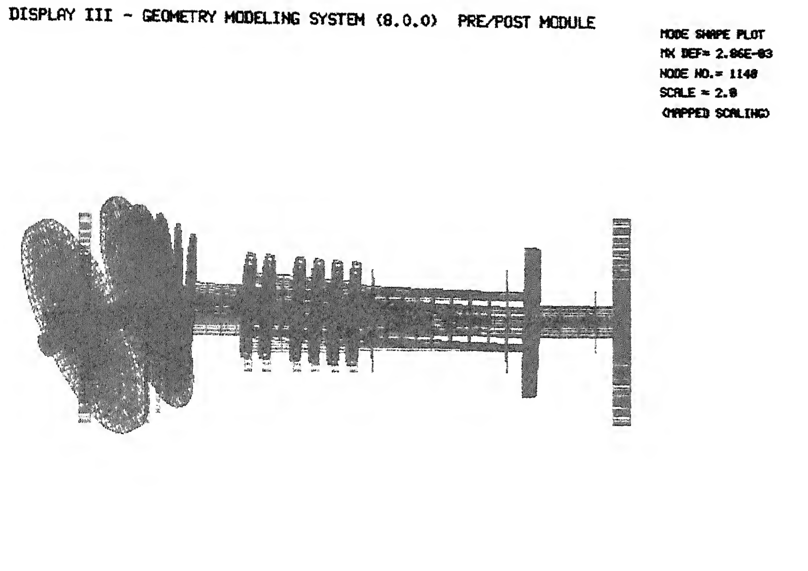

(a)

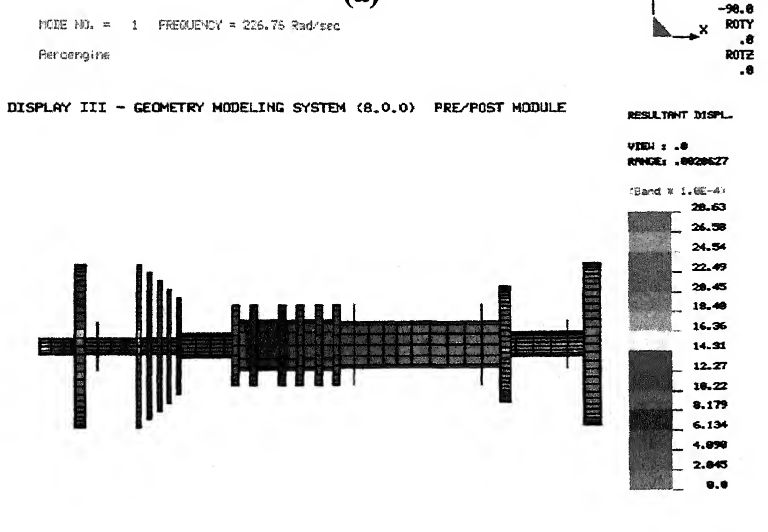

(b)

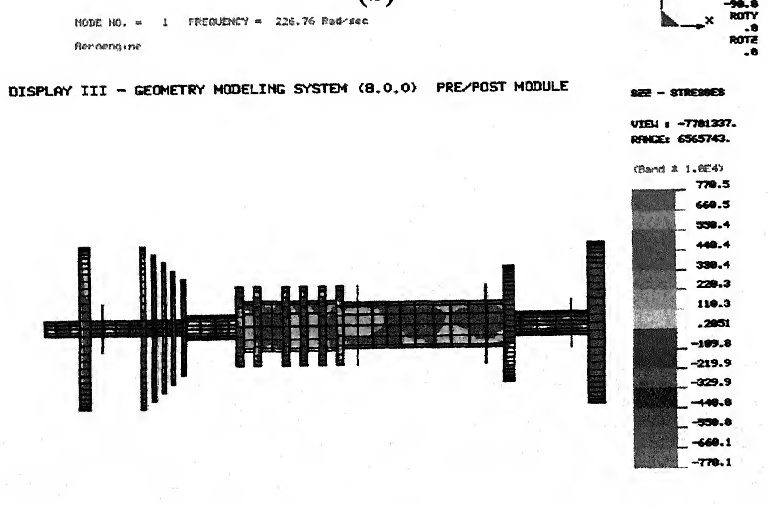

(c)

Figure 4.3 **I Mode of Aeroengine Rotor**
(a) Modeshape
(b) Displacement Contours
(c) Stress Contours

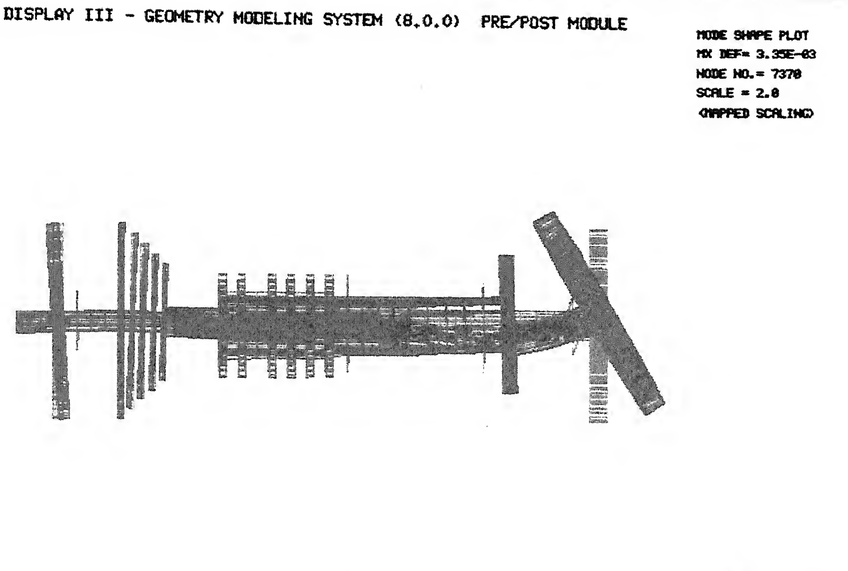

(a)

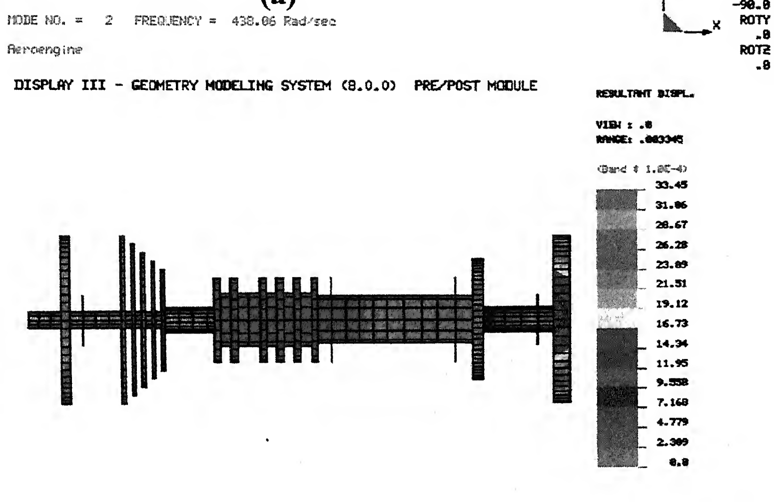

(b)

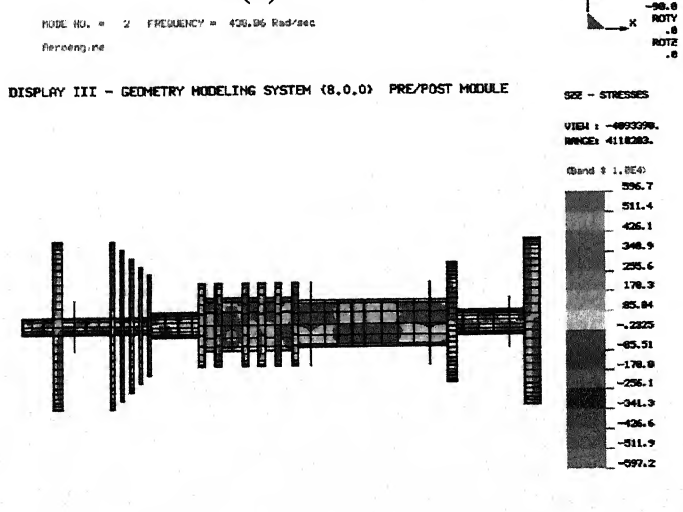

(c)

Figure 4.4 **II Mode of Aeroengine Rotor**
(a) Modeshape
(b) Displacement Contours
(c) Stress Contours

Table 4.4 Natural Frequencies (rad/s.) of Aeroengine rotor

Transfer Matrix Method	FEM model
226.00	226.76
424.00	438.06
443.00	489.58
717.00	572.16

Fig. 4.3 shows the modeshape corresponding to the first natural frequency of transverse vibration, This figure also includes the contour plot of resultant displacement and stress in aeroengine rotor for first natural frequency. Similarly the Fig. 4.4 and Fig 4.5 shows the modeshape corresponding to second and third transverse natural frequency respectively. Critical speeds of aeroengine rotor for forward and backward synchronous with inner and outer rotor are given in Table 4.5.

Table 4.5 Critical speeds (rad/s) of Aeroengine rotor

Synchronous Whirl with inner rotor		Synchronous whirl with outer rotor	
Forward Whirl	Backward Whirl	Forward whirl	Backward Whirl
312	172	282	186
764	295	667	325
1104	337	781	358
1544	563	1255	604

4.4 Residual Unbalance Response

The unbalance responses of aeroengine rotor at different speed ratios are obtained by extended transfer matrix method. Rotors in an aeroengine rotor are balanced at regular maintenance intervals. However, some residual unbalance still remains, depending on the quality of balancing achieved. Unbalance response has been computed here, for such typical residual unbalance, which is listed in Table 4.6. Whirl orbit for inner and outer rotors have been obtained for three different speed ratios. Fig 4.6 shows the whirl orbits at the speed ratio of 2500rpm/2000rpm, 3500rpm/3000rpm and 4500rpm/4000rpm. The time period of whirl was found to be 0.12 s, with 5,7 and 9 loops for first, second and third set of speed ratio respectively from equations 3.34 and 3.35. The whirl orbits have been plotted at the fourth stage of LP compressor for inner rotor and at the third stage of HP compressor for outer rotor.

Table 4.6 Unbalance on Aeroengine rotor

Component Name	Stage No.	Unbalance ($m_i e_i$) Kg.m	Angle of eccentricity (β_i)
Inlet vane	-	0.0372	20.0
L.P. Compressor	1	0.0180	10.0
	2	0.0110	5.50
	3	0.0080	4.00
	4	0.0060	3.00
	5	0.0110	5.50
H.P. Compressor	1	1.200	6.0
	2	1.200	6.0
	3	1.200	6.0
	4	1.200	6.0
	5	1.200	6.0
	6	1.600	8.0
L.P. Turbine	1	0.063	31.5
H.P. Turbine	1	0.880	4.50

The whirl orbits for the various stages along the rotor length at the speed ratio of 2500rpm/2000rpm are shown in Fig. 4.7 (a)-(b). The plot however, does not correctly represent the relative orientation of the orbits of the various stages. The dynamic displacements at various stages, along the rotor, at one particular time instant, have been shown joined by straight lines, in the figure. From Fig 4.7 (a)-(b) one can visualize that at given speed ratio of 2500rpm/2000rpm, which is close to first natural frequency of aeroengine rotor the mode of vibration of inner and outer rotor is very close to first modeshape of aeroengine (Fig 4.4) .Better post-processing of results is required for a more realistic spatial representation of the rotor response. The exercise is however, sufficient, to highlight the fact that aeroengine rotor dynamics, is a function of a variety of design and operating parameters and a rigorous parametric study is essential to draw meaningful inferences.

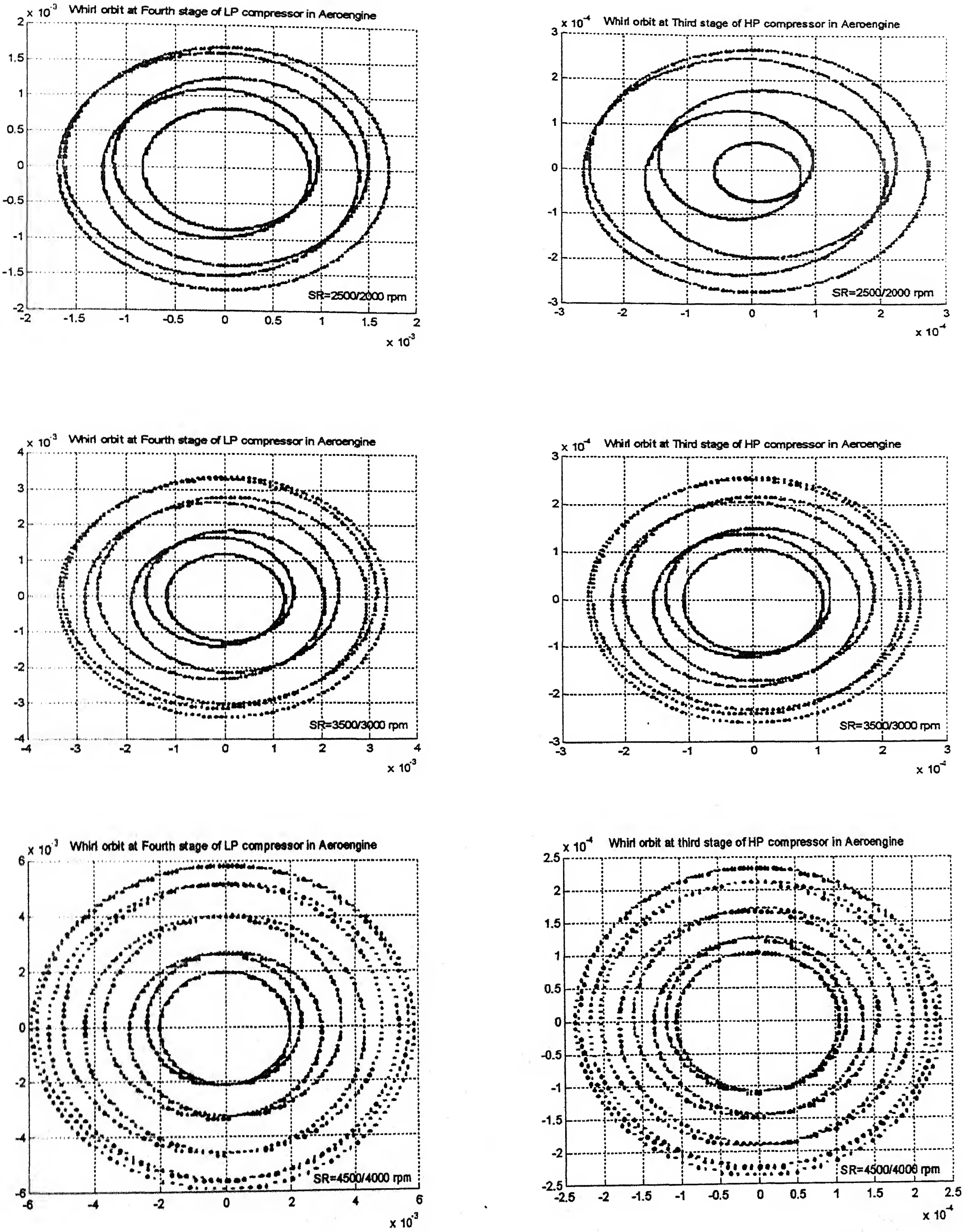

igure 4.6 Whirl orbits at fourth LP stage and third HP stage of aeroengine.compressor

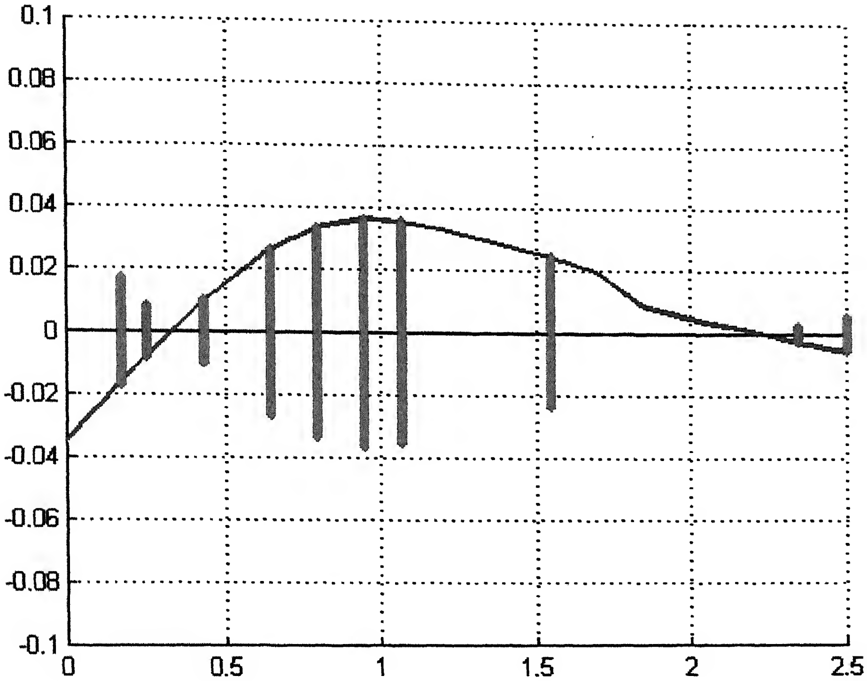

(I)

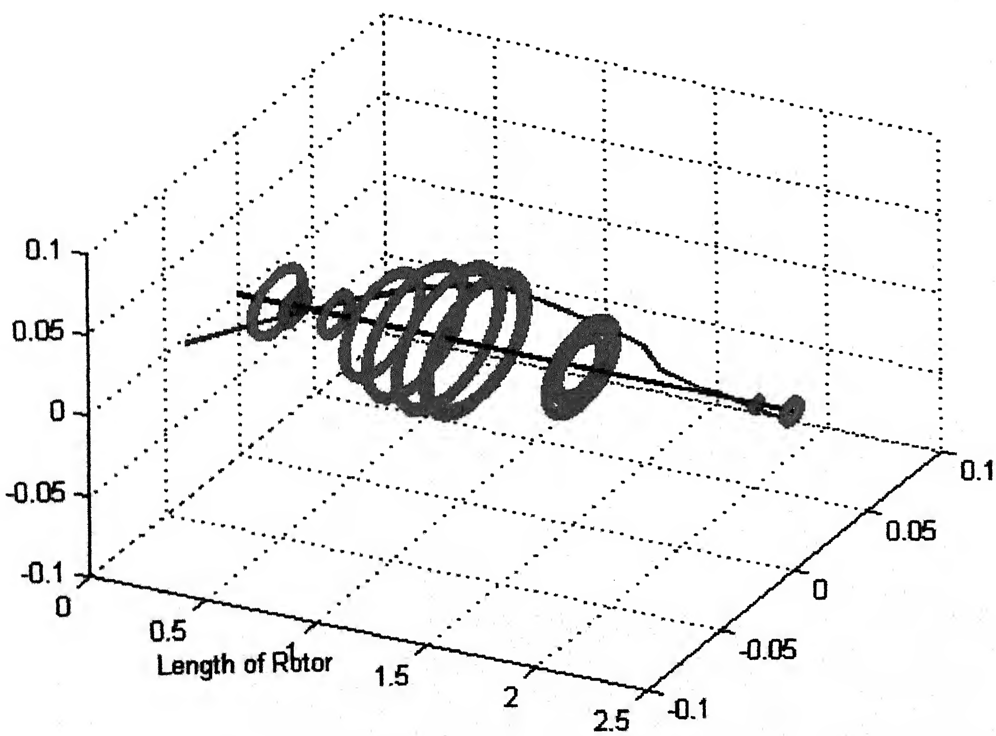

(II)

Figure 4.7(a) Whirl orbits along the inner rotor

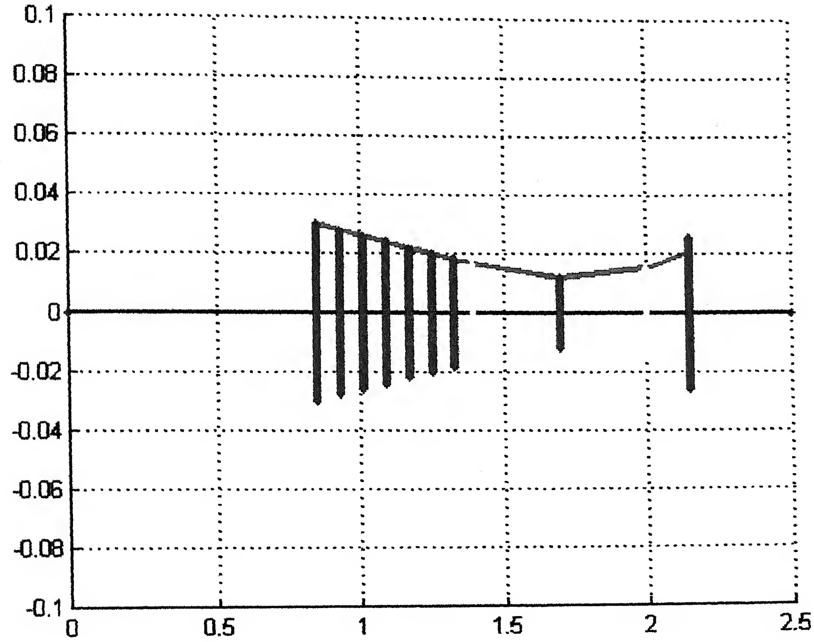

(I)

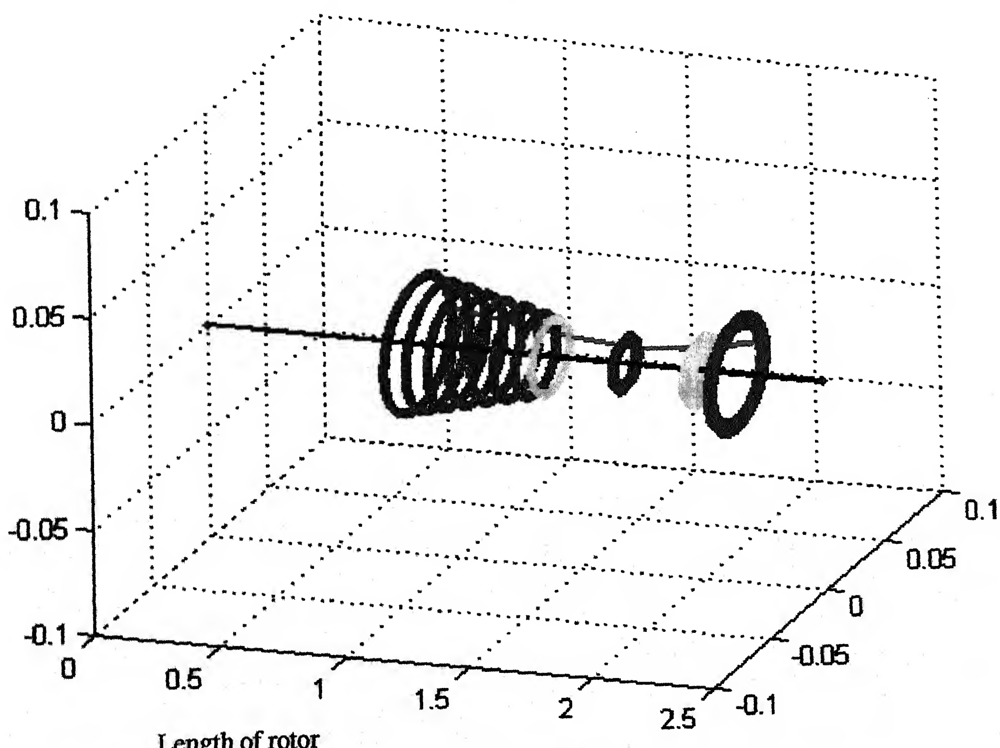

(II)

Figure 4.7(b) **Whirl orbits along the outer rotor**

CHAPTER 5

CONCLUSIONS AND SCOPE FOR FUTURE WORK

Models and algorithms have been developed during the course of this study for dynamic analysis of dual and multi-spool rotors. The basic features of such rotors are rotating shafts, which support other rotating shafts through intershaft bearings. This arrangement, while improving upon the compactness of the installation makes its dynamic behaviour more complex by introducing additional coupling influences of intershaft bearings. The transfer matrix models account for such inter-component interactions in a simple and efficient manner. However, the accuracy of results is a function to the discretisation adopted. Modeling of rotating components is difficult in most finite element software packages. The difficulty is compounded in the case of dual rotors, with shafts rotating at different speeds. Keeping these limitations in view, modeling was attempted in NISA software package in order to appropriately model intershaft connections and obtain better visualisation of the complex mode shapes. These models could be successfully developed. The results for standard problems available in literature were obtained to validate the models. Gyroscopic effects were included in the transfer matrix algorithms and critical speeds have been calculated for forward and backward whirls synchronous with speeds of different rotors. A chart for nonsynchronous whirl as function of rotating speeds is also generated. Modeling and analysis has been carried out also for an aeroengine rotor. Stiffness calculation for typical rolling element bearings has been carried out.

The present models establish the framework for detailed parametric studies on dual rotor dynamics. Influence of various intershaft stiffness parameters needs to be investigated in more detail. This can include both direct stiffness and cross-stiffness terms. Influence of damping can also be studied with the help of present computer programs. Influence and location of other bearings on the inner and outer shafts can

be studied in terms of nondimensional parameters. Rigorous studies can also be conducted to investigate the coupling influences at different speed ratios. Experimental investigations can also be carried out, by building simple laboratory models, to validate the computational results and investigate other phenomenon like instability in dual rotors.

REFERENCES

1. Dimentberg, M. F., *Flexural vibrations of rotating shafts,* Butterworthes, London, 1961.
2. Tondal, A., *Some problems of rotor Dynamics*, Chapman and Hall, London, 1965.
3. Rao, J. S., *Rotor Dynamics*, Third edition, New Age International (P) Limited, New Delhi, 1996.
4. Myklestad, N. O., *A new method of calculating natural modes of uncoupled vibrations of airplane wings and other types of beams*, J. Aero Sc., 1944.
5. Prohl, M. A., *A general method for calculating critical speeds of flexible rotors*, Trans. ASME, 1945.
6. Kikuchi, K., *Analysis of unbalance vibration of rotating shaft with many bearings and discs*, Bull. JSME, Vol. 13., No. 61, 1970.
7. Green, R. B., *Gyroscopic effects on critical speeds of flexible rotors*, J. of Appld. Mechs., ASME Vol. 15, 1958.
8. Carnegie, W., *Rotary inertia and gyroscopic effects in overhung Shaft system*, Bull. Mech. Engg. Edu., Vol. 3, 1964.
9. Smith, D. M., *Journal bearings in turomachinery,* Champman and Hall Ltd., 1969.
10. Lund, J. W., *Rotor bearings dynamic design technology* part-3: Design handbook for fluid film bearings, Mechanical Technology Inc., AFAPL-Tr-65-45, 1965
11. Morton, P.G., Johnson, J. H. and Wale, G. D., *The effects of thermal distortions on the characteristics of large hydrodynamic bearings*, Proc. Instn. of Mech. Engrs., Vol. 202, C3, 1988, pp. 219
12. Goodwin, M.J., *Dynamics of rotor-bearing system*, Unwin Hyman, London, 1955
13. Gupta, K. D., *et al.*, *Dynamic response of a dual-rotor system by extended transfer matrix method*, Proc. I. Mech. E. Intl. Conf. On vibrations in rotating Machinery, U.K., pp. 599
14. Gupta, K., *et al.*, *Unbalance Response of a dual rotor System: Theory and Experiment*, J. of Vibration and Acoustics., Vol. 115, 1993 pp. 427

15. Rajan, M., Nelson, H.D., and Chen, W.J., *Parameter Sensitivity in the Dynamics of Rotor-Bearing Systems*, J. of Vibration, Acoustics, Stress and Reliability in Design., Vol. 108, 1986, pp. 197
16. Taiping, H., *The Transfer Matrix Impedance Coupling Method for the Eigensolutions of Multi-Spool Rotor Systems*, J. of Vibration, Acoustics, Stress and Reliability in Design., Vol. 110, 1988,pp. 469
17. Harris, T. A., *Rolling Bearing Analysis*, John Wiley & Sons, Inc., New York, 1966.
18. Ragulskis, K. M., *et al.*, *Vibration of Bearings*, Oxonian Press Pvt. Ltd., New Delhi, 1979.
19. Rossing, T.D. and Fletcher, N. H., *Principles of vibration and sound*, Springer-Verlag, New York, 1995.
20. Pestel, E. C. and Leckie, F. A., *Matrix method in elastomechanics*, McGraw-Hill Book Co., 1958.
21. Thomson, W. T., *Theory of vibration with applications*, Unwin Hyman Ltd., London, 1988.
22. Mahadevan, K. and Balaveera Reddy, K., *Design data hand book for Mechanical Engg.*, Third Edition, CBS, 1998.
23. Tiwari, R., and Vyas, N. S., *Parameter estimation in imbalanced non-linear rotor bearing systems form random response*, J. of Sound and Vibration, Vol. 208, 1997.
24. Tiwari, R., and Vyas, N. S., *Stiffness estimation from random response in multi-mass rotor bearing systems*, Prob. Engg. Mech., Vol. 13 No. 4, pp-255, 1998

A133644

Date Slip

The book is to be returned on the date last stamped.
